9-12-2003

# Modeling and Simulation of Steering Systems for Autonomous Vehicles

Shailesh Lakkad
*Florida State University*

THE FLORIDA STATE UNIVERSITY

COLLEGE OF ENGINEERING

# MODELING AND SIMULATION OF STEERING SYSTEMS FOR AUTONOMOUS VEHICLES

By

SHAILESH LAKKAD

A Thesis submitted to the
Department of Mechanical Engineering
in partial fulfillment of the
requirements for the degree of
Master of Science

Degree Awarded:
Spring Semester, 2004

The members of the committee approve the thesis of Shailesh Lakkad, defended on Sept 12, 2003.

_____
Patrick Hollis,
Professor Directing Thesis

_____
Carl Moore,
Committee member

_____
Rodney Roberts,
Committee member

Approved:

_____
Chiang Shih, Chair, Ph.D., Department of Mechanical Engineering

_____
C. J. Chen, Ph.D., Dean, FAMU- FSU College of Engineering

The office of Graduate Studies has verified and approved the above named committee members.

## ACKNOWLEDGEMENT

I would like to take this opportunity to thank a few of the many people who have made my graduate studies and this thesis possible. To them and many others I am truly grateful. First of all, I would like to express my deepest gratitude to my advisor, Dr. Patrick Hollis for his technical guidance and financial support throughout my research. I found my research and work place so enjoyable because of his invaluable supervision and constant encouragement.

I would also like to thank Dr. Carl Moore and Dr. Rodney Roberts for serving in my graduate committee and for introducing me to the world of robotics. Special thanks to financial support provided by robotics research lab at FAMU-FSU without which this thesis wouldn't be possible. I am thankful to Dr. Farrukh Alvi (Graduate Coordinator) for providing me an opportunity to study in Graduate school at Florida State University.

I owe special gratitude to Pankaj, Debangshu, and Deviprasad for being such nice friends and for helping in my research. They were of immense help and support to me. They made my stay in Tallahassee very pleasant and rich. I feel very privileged to have worked with so many nice people at Florida State University.

I feel most indebted to my brother Yogesh, who taught me the importance of education in life and to my father and mother who gave me the courage to face and overcome new challenges. It wouldn't have been possible to come to U.S.A. for graduate studies without love and support of Chitragupt, Sachin, Amol , Chintamani, Shripad and Pankaj. Without them none of my dreams would have become reality. This thesis is dedicated to all these most important people in my life.

## TABLE OF CONTENTS

## LIST OF FIGURES

## NOMENCLATURE

| | |
|---|---|
| $F_{yf}$ | lateral force at front tire |
| $F_{yr}$ | lateral force at rear tires |
| $U_x$ | longitudinal Velocity |
| $U_y$ | lateral velocity |
| $\alpha_f$ | front tire slip angle |
| $\alpha_r$ | rear tire slip angle |
| $C_f$ | front tire cornering stiffness |
| $C_r$ | rear tire cornering stiffness |
| $\delta_f$ | front steering angle |
| $\delta_r$ | rear steering angle |
| $a$ | front tire distance from CG along longitudinal axis |
| $b$ | rear tire distance from CG along longitudinal axis |
| $I_z$ | yaw moment of inertia of vehicle |
| $m$ | mass of vehicle |
| $r$ | yaw rate |
| $a_y$ | lateral acceleration |
| $I_s$ | equivalent moment of inertia of steering |
| $C_s$ | equivalent damping coefficient of steering system |
| $N_t$ | steering gear ratio |

| | |
|---|---|
| $N_m$ | motor gear ratio |
| $\xi$ | trail of front tire |
| $\beta$ | vehicle heading angle |
| $K_m$ | torque constants |
| $K_b$ | back e.m.f. constant |
| $J$ | back e. m. f. constant |
| $R$ | coil resistance |
| $L$ | coil inductance |
| $T_d$ | disturbance torque |
| $N$ | yawing moment |

## ABSTRACT

Robotic tasks call for a range of steering activity: one extreme is highway driving with negligible turning for hundreds of kilometers; another is steering for battlefield robots, which call for agile turning. System modeling and simulation are more widely used in robotic vehicle engineering to reduce development time, improve the design and miniaturization of complex systems. This thesis research mainly focuses on steering system modeling and simulation. It also reviews different steering schemes that are used for robotic vehicles and battlefield robot vehicles such as the XUV. Steering systems that are modeled and simulated are skid steering and four wheel steering. A dynamic model is developed for a skid steered robot ATRV-Jr considering lateral forces and longitudinal resistance. It is followed by a Matlab simulation of the state variables. Results of the Matlab simulation are compared to the results obtained from ADAMS simulation of the solid model of the ATRV-Jr. Then the concept of four wheel steering is introduced for the XUV. A basic steering system model is developed using steering system dynamics for four wheel steering. A Matlab simulation of this model is done to check the stability of the system. It is followed by vehicle handling characteristics of the XUV for the four-wheel steering system and its Matlab simulation. Finally, a four-wheel steering model of XUV is developed in ADAMS for dynamic motion analysis. The results of dynamic motion analysis are discussed for future research.

# CHAPTER 1

# INTRODUCTION AND FUNDAMENTALS OF STEERING

## 1.1 Introduction

Mobile Robotics research can be divided into the following potential areas:

1) Advanced Perception
2) Advanced Control Architecture
3) Vehicle Dynamic Modeling, Simulation and Experimentation

The research focus in this thesis is on dynamic modeling, 3D solid modeling, and simulation. Pro-E and ADAMS are used extensively for 3D solid modeling and dynamic simulation. Matlab and Simulink are used for theoretical simulation. A prototype robot called the ATRV-Jr is used for validating some the results from theoretical simulation.

This Research involves three sections:

1) Dynamic Modeling and Simulation of prototype robot ATRV-Jr
2) Modeling and Analysis of four wheel steering for XUV
3) Computer Simulation of Four wheel steering

Steering geometry and various configurations of possible steering mechanisms are discussed. Various steering schemes are compared on the basis of maneuverability, power requirements, control system requirements, etc. It is followed by dynamic modeling of skid steered robot such as the ATRV-Jr. A Matlab simulation is performed and the results are compared with a dynamic analysis using ADAMS. Chapter 4 discusses some of the ideas for 4 wheel steering which can be used on the XUV. Chapter 5 is

devoted to the steering system dynamics and a relation between steering angle and input voltage is developed. Vehicle handling characteristics are discussed in next section and finally a four wheel steered model and it's dynamic analysis using ADAMS is discussed.

### 1.2 Fundamentals of Steering

This section examines fundamentals of steering and the concept of Instantaneous Center of Rotation.

Figure 1.1 shows instantaneous position of a four-wheeled vehicle.

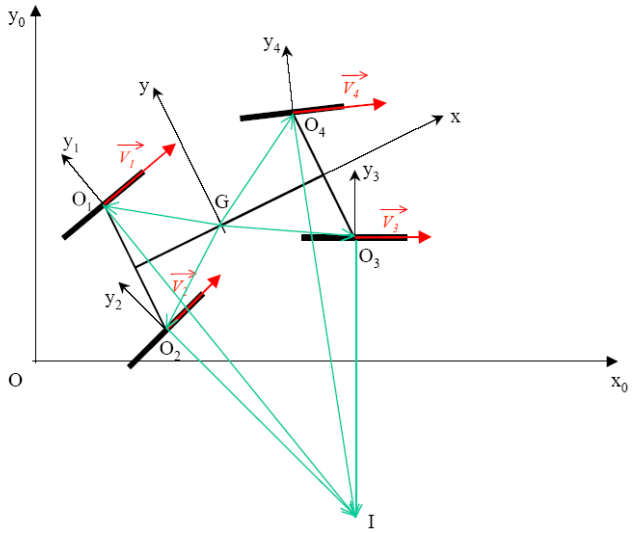


Figure 1.1 ICR concept

Wheel axes must intersect at a point if there is no slipping. This point, I, is the Instant Rotation Center (IRC) for vehicle movement relative to the surface.

### 1.1 Three-wheeled robot steering study

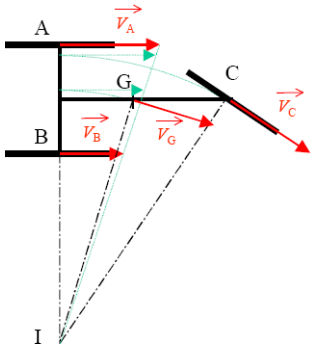


Figure 1.2 Three-wheeled mobile robot steering

We assume that there is no slip. Each wheel velocity is perpendicular to its rotation axis. In this case, wheels A and B have the same rotation axis. The IRC is situated at the intersection of A (or B) and C wheel axes. Note that $V_A \neq V_B \neq V_C$, so the three wheels have to be independent to rotate at different velocities. This means that if the three-wheeler is a rear wheel drive, a differential is needed between the rear wheels. If there are three driving wheels, a second differential is required between front and rear.

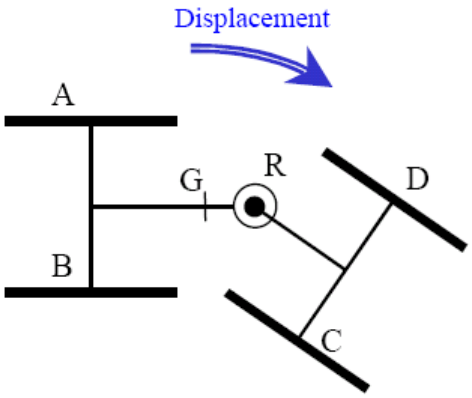


Figure 1.3 Trailer like vehicle steering

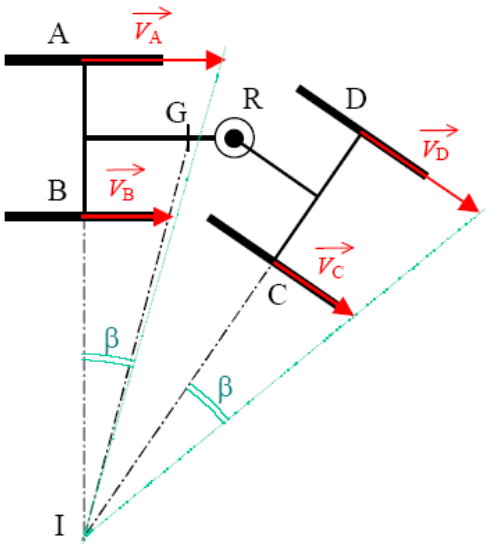


Figure1.4 Geometric analysis

**1.2 Trailer like vehicle steering study (Fig. 1.4)**

In this case, wheels A - B and C - D have the same rotation axis. The IRC is situated at the intersection of A (or B) and C (or D) wheel axes. Note: $V_A \neq V_B \neq V_C \neq V_D$, so the four wheels have to be independent to be able to rotate at different velocities. This means that if the vehicle is a rear wheel drive, a differential is needed between the rear wheels. If it is a four-wheel drive, two more differentials are required.

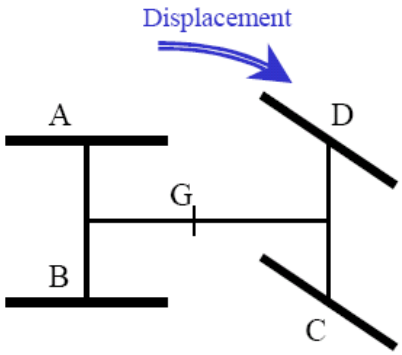


Fig 1.5 Four wheeled, two steering wheels

### 1.3 Four-wheeled, two steering wheels study

If the steering wheels remain parallel during steering as shown in Figure 1.6, there is no single intersection point; this is incompatible with the no slip hypothesis. In this case, at least one velocity vector must have a different direction. This implies that at least one wheel slips to allow the vehicle to move. A solution is to use a different steering angle for each steering wheel. The angle between steering wheels is called Ackermann angle.

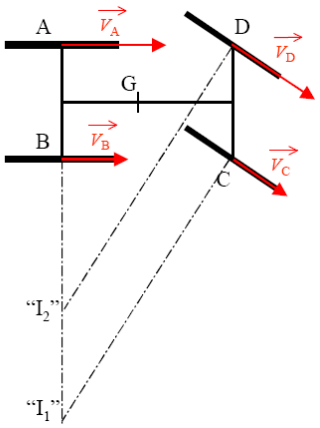


Figure 1.6 Parallel steering kinematic study

### 1.4 Non Parallel Steering wheels

With a correct differential steering angle, the IRC exists and can be found the same way as previously. The IRC is situated at the intersection of A (or B) and C (or D) wheel axes. Because of the perfect grip, the differential steering angle must be such that the three wheel axes intersect at the same point (the IRC). Note: the 4 wheels have to be independent to be able to rotate at different velocities. This means that if the vehicle is a rear-wheel drive, a differential is needed between the rear wheels. If it has four-wheel drive, two more differentials are required.

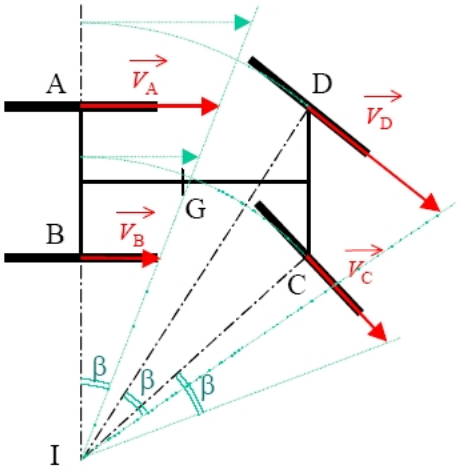

Figure 1.7 Non parallel steering

### 1.5 Four wheeled vehicle with four steering wheel

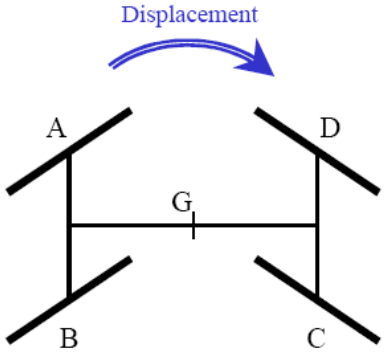

Figure 1.8 Four-wheeled vehicle with four steered wheels

### 1.6 Parallel Steering study

If the steering wheels remain parallel during steering (Figure 1.9), there is no single intersection point. This is incompatible with the no slip hypothesis. In this case, at least two velocity vectors must have a different direction. This implies that at least two wheels slip to allow the vehicle to move. A solution using a different steering angle for each steering wheel can be used. The angle between the steering wheels is called the Ackerman angle.

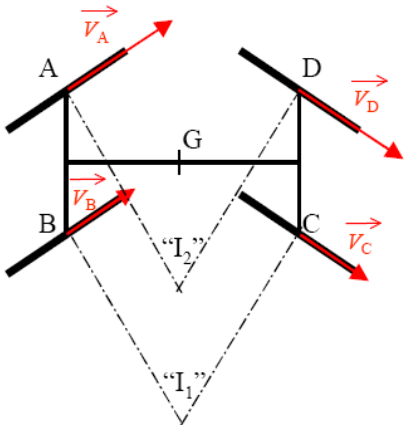


Figure 1.9 Four-wheeled vehicle with parallel steering

### 1.7 Nonparallel Steering

With correct steering angles, the IRC exists and can be found. Compared to the previous case, this kind of steering (Figure 1.10) permits an IRC to be located anywhere in the plane. Again, the differential steering angle must be correct.

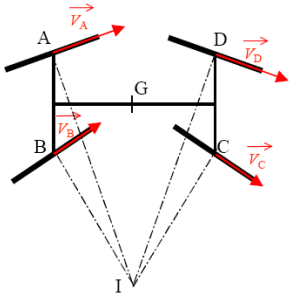


Figure 1.10 Four-wheeled vehicle with nonparallel steering

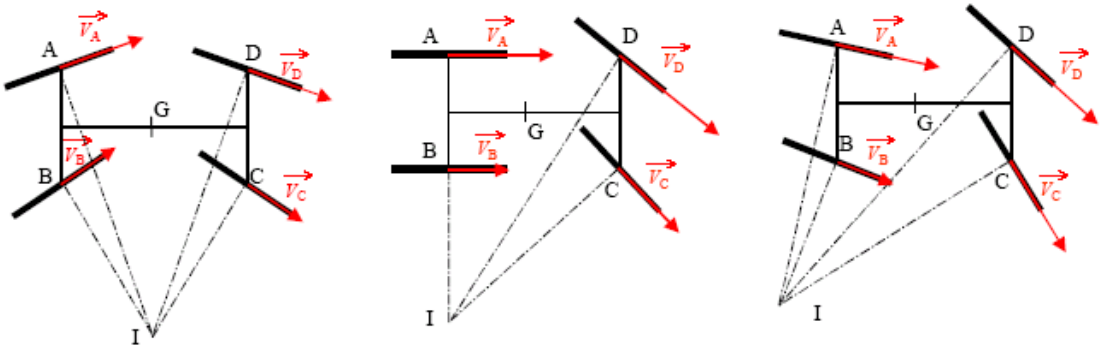


Figure 1.11 Arbitrary IRC location for nonparallel steering

There are some special cases that warrant separate attention .

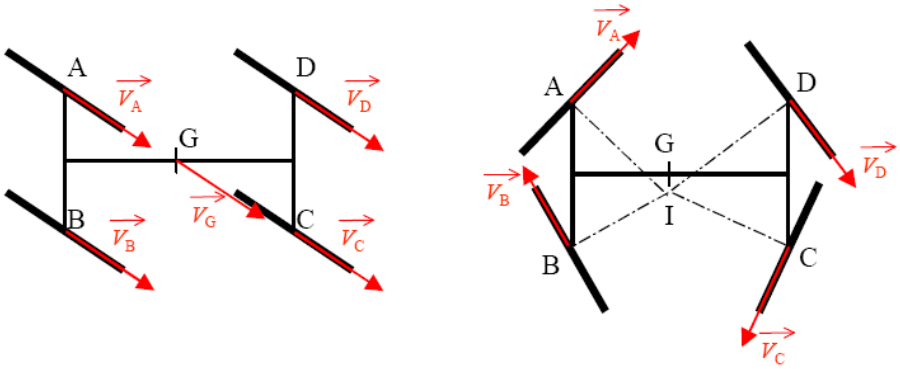


Figure 1.12 Special cases of nonparallel steering

### 1.8 Steering System for XUV

An XUV type vehicle is used for reconnaissance, combat operations, and operation on unprepared terrain. Terrain could vary from ice to mud or sand. Steering schemes that can be considered are

1) Independent (explicit) steering: Independent steering explicitly articulates each of the wheels to the desired heading. Apart from the issues of actuation complexity and accuracy of coordination control, this scheme provides advantages to the maneuverability of mobile robots, especially those operating in unprepared terrains. A common variation of independent all-wheel steering, not attainable by the other schemes, is crab steering in which all wheels turn by the same amount in the same direction. As a result, the robot can move in a sideways fashion. Coordination of driving and steering allows efficient maneuvering and reduces the effect of internal losses due to actuator fighting.

2) Ackerman Steering: The most common type of steering on passenger cars is Ackerman steering that mechanically coordinates the angle of the front two wheels. In order to maintain all wheels in a pure rolling condition during a turn the wheels need to follow curved paths with different radii originating from a common center. Advantages of explicit steering include more aggressive steering with better dead reckoning (due to less slip of the wheels) and lower power consumption. The downside of explicit steering is a higher actuator count, part count, and the necessary swept volume. Articulated frame steering is prevalent in large earth moving equipment. The heading of the vehicle changes by folding the hinged chassis units. For large vehicles, articulated frame steering has the advantage of allowing the vehicle to be significantly more maneuverable than a vehicle with coordinated steering. Articulated frame steering has the advantage over skid steering in that during a turn the maximum thrust provided by the traction elements is maintained.

3) Skid steering: Skid steering can be compact, light, require few parts, and exhibit agility from point turning to line driving using only the motions, components, and swept volume needed for straight driving. Skid steering is achieved by creating a differential thrust between the left and right sides of the vehicle thus causing a change in heading. This is an

effective and easy solution to steering the robot. However, it is not as accurate as other steering methods; certain characteristics including friction, wheel slippage and other unpredictable attributes can cause problems. This steering configuration is a special case where the bisectors of the wheels do not intersect and wheel slip is exploited to cause the robot to rotate. The downside is that skidding causes unpredictable power requirements because of terrain irregularities and non-linear tire-soil interaction. Skid steering also fails to achieve the most aggressive steering possible, which can be achieved with explicit steering because the maximum forward thrust is not maintained during a turn.

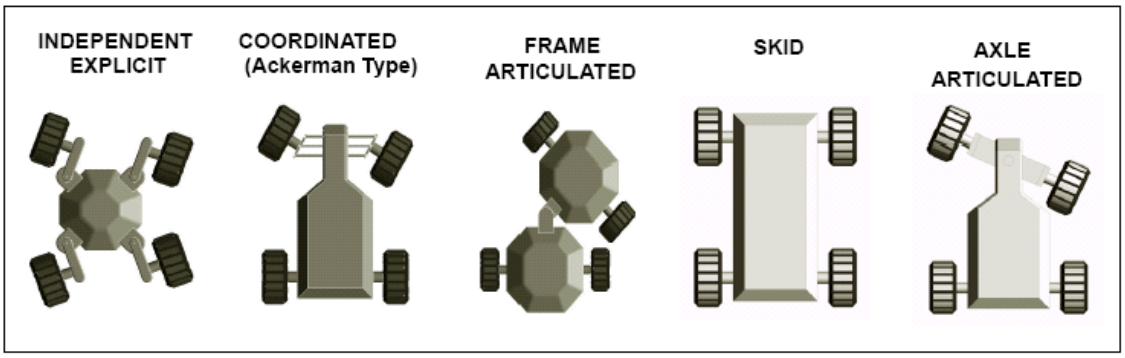


Figure 1.13: Kinematics of major steering types (Source: Ref 10)

4) Passively articulated axle: This type of steering is performed by adding a free pivot to one of the vehicle axles. It is commonly found in wagons or carts. One disadvantage of single axle steering is that the wheels run in separate tracks when going around curves. Under difficult ground conditions this requires increased drive propulsion as each wheel is driving over fresh terrain. The advantages include mechanical simplicity, relatively low steering power, and moderate maneuverability.

Table A shows a comparison of all types of steering based on parameters such maneuverability, mechanical complexity, control system requirements etc.

Table A Steering system evaluation for XUV

| | Independent Explicit | Coordinated Ackerman | Frame Articulated | Skid | Axle Articulated |
|---|---|---|---|---|---|
| Maneuverability | med/high | med | med | high | med |
| Mechanical complexity | med | med/high | low | low | low |
| Control complexity | low | med/low | med | low | med/high |
| Power | med | med/low | med | high | low |
| Number of joints for steering | 4 | 1 | 1 | 0 | 0 |

## CHAPTER 2

## DYNAMIC MODELING OF SKID STEERED VEHICLE

Dynamic modeling and simulation plays a critical role in the engineering of robotic control code, and there exist a variety of strategies for both building physical models and for interfacing with theses models. The development of kinematic and dynamic models of vehicle motion is crucial in the design of vehicle navigation and control systems. Models must reflect kinematic and dynamic properties such as vehicle slip and traction effects in land vehicles, AGV's etc. The development of mathematical models that allow estimation of the traction conditions that exist between a vehicle tire and a road surface forms the basis for theoretical simulation modeling. The ATRV-Jr. used for modeling and simulation is a 4 wheel differentially driven (4wdd) vehicle in which rotational motion is achieved by a differential thrust on wheel pairs at opposite sides. A dynamic model is described using the standard bicycle model (3 degrees of freedom).

We do not focus on real time control since our objective was to model and validate the skid steered vehicle in simulation and experimental set up.

Figure 2.1 – iRobot ATRV-Jr (Source : iRobot Corporation )

## 2.1 Dynamic Modeling

We develop a vehicle dynamic model by neglecting some effects introduced by suspension and tire deformation. We follow the standard SAE vehicle axis system as shown in figure 2.2.

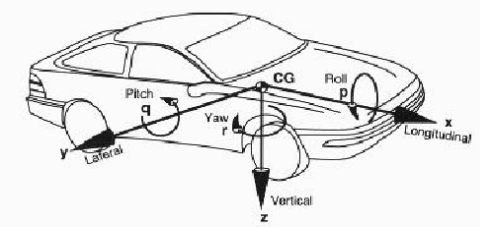


Figure 2.2 Vehicle axis system

## 2.2 Equations of Motion

The following assumptions are made:

1) Vehicle is moving on the horizontal plane
2) Vehicle speed is very low
3) Longitudinal slippage neglected
4) Lateral force of the tire is directly proportional to its vertical load
5) Wheel actuation is equal on each side to reduce longitudinal slip
6) Vehicle is rotating counterclockwise

Referring to figure 2.3, *O(X,Y)* defines a fixed reference frame and *O(x,y)* is a moving frame attached to the vehicle body with origin at the center of mass. The center of mass is located at distances *a* and *b* from front and rear wheels respectively. Wheelbase is 2*t*.

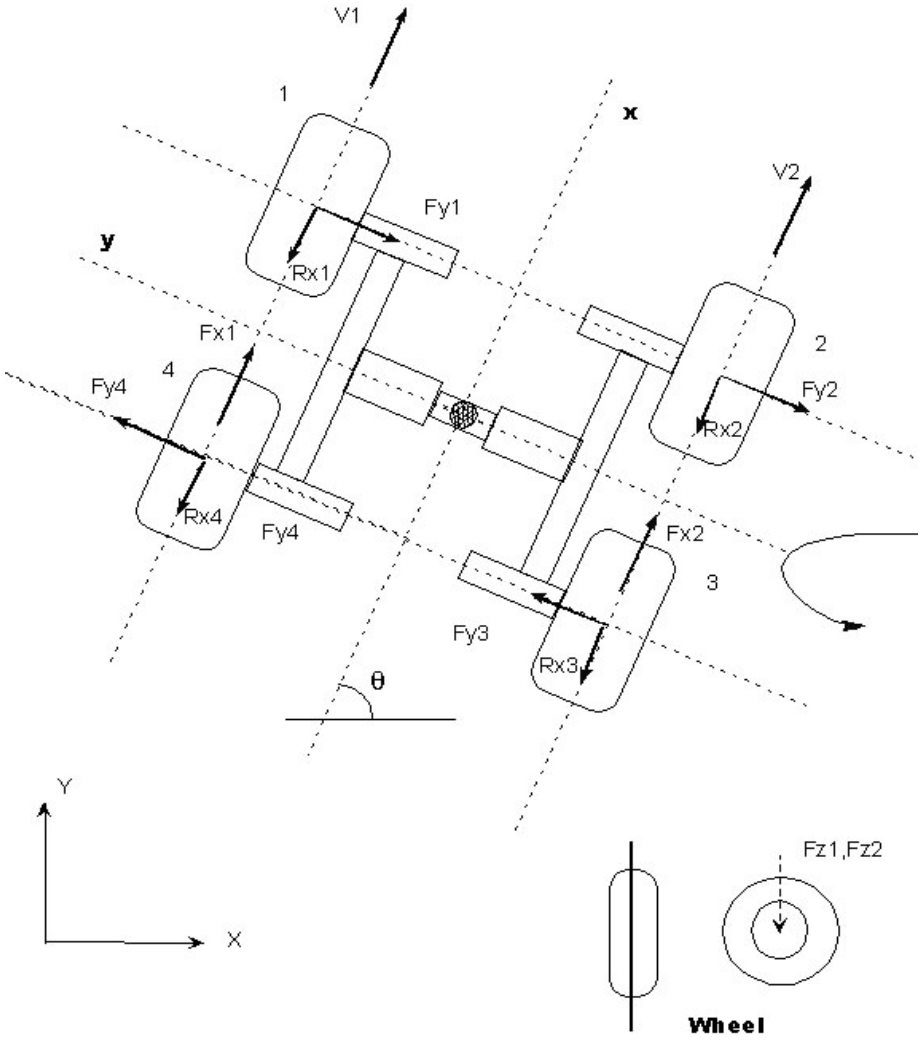


Figure 2.3 Free body diagram for ATRV-Jr.

$\theta = \text{Angle of } x\text{–axis with } X\text{-axis}$

Then the rotation matrix relating the coordinate frames is given by

$$R(\theta) = \begin{bmatrix} \cos\theta & \sin\theta \\ -\sin\theta & \cos\theta \end{bmatrix}$$

Let $\dot{x}, \dot{y}, \dot{\theta}$ be the longitudinal, lateral and angular velocity of the vehicle in local frame *f*. In the fixed frame *F*, the absolute velocities are

$$\begin{bmatrix} \dot{X} \\ \dot{Y} \end{bmatrix} = \begin{bmatrix} \cos\theta & \sin\theta \\ -\sin\theta & \cos\theta \end{bmatrix} \begin{bmatrix} \dot{x} \\ \dot{y} \end{bmatrix}$$

Differentiating w.r.t. time gives the acceleration,

$$\begin{bmatrix} \ddot{X} \\ \ddot{Y} \end{bmatrix} = \begin{bmatrix} \cos\theta & \sin\theta \\ -\sin\theta & \cos\theta \end{bmatrix} \begin{bmatrix} \ddot{x} + \dot{y}\dot{\theta} \\ \ddot{y} - \dot{x}\dot{\theta} \end{bmatrix} = R(\theta) \begin{bmatrix} a_x \\ a_y \end{bmatrix}$$

The longitudinal velocity $x_i$ and lateral velocity $y_i$ are given by

$$\begin{aligned} \dot{x}_1 &= \dot{x}_4 = \dot{x} - t\dot{\theta} \qquad (left) \\ \dot{x}_2 &= \dot{x}_3 = \dot{x} + t\dot{\theta} \qquad (right) \\ \dot{y}_1 &= \dot{y}_2 = \dot{y} + a\dot{\theta} \qquad (front) \\ \dot{y}_3 &= \dot{y}_{14} = \dot{y} - b\dot{\theta} \qquad (front) \end{aligned} \tag{1}$$

The free body diagram of forces and velocities is shown in figure 2.3. The vehicle has velocities $\dot{x}$, $\dot{y}$, and $\dot{\theta}$. Wheels develop tractive forces $F_{xi}$ and are subject to rolling resistances $R_{xi}$ where $i = 1, 2, 3, 4$. As wheel actuation is equal, $F_{x1} = F_{x4}$ and $F_{x2} = F_{x3}$. Lateral forces $F_{yi}$ acts against lateral skidding and there is a resistive moment $M_r$ about the center of mass due to $F_{yi}$ and $R_{xi}$. For a vehicle of mass *m* and moment of inertia *I*, the equations of motion in frame *f* can be written as follows

$$\begin{aligned} ma_x &= 2F_{x1} + 2F_{x2} - R_x \\ ma_y &= -F_y \\ I\ddot{\theta} &= 2t(F_{x1} - F_{x2}) - M_r \end{aligned} \tag{2}$$

When the vehicle is at rest,

$$F_{z1} = F_{z2} = \frac{b}{a+b}\frac{mg}{2}$$
$$F_{z3} = F_{z4} = \frac{a}{a+b}\frac{mg}{2}$$

At low speed, the lateral load transfer due to centrifugal forces can be neglected. For hard ground, the contact patch between the tire and wheel can be assumed to be rectangular and hence has a uniform pressure distribution. In this condition, $R_{xi} = f_r F_{zi}\,\mathrm{sgn}(\dot{x}_i)$ where $f_r$ is the coefficient of rolling resistance assumed to independent of velocity [7].

$$R_x = \sum_1^4 f_r F_{zi}\,\mathrm{sgn}(\dot{x}_i) = f_r \frac{mg}{2}\left(\mathrm{sgn}(\dot{x}_1) + \mathrm{sgn}(\dot{x}_2)\right)$$

Considering the Coulomb friction model for the wheel ground contact, the lateral force on each wheel is $F_{yi} = \mu F_{zi}\,\mathrm{sgn}(\dot{y}_i)$ where $\mu$ is lateral friction coefficient. The total lateral force is

$$F_y = \sum_1^4 f_r F_{zi}\,\mathrm{sgn}(\dot{y}_i) = \mu \frac{mg}{2}\left(\mathrm{sgn}(\dot{y}_1) + \mathrm{sgn}(\dot{y}_3)\right)$$

The resistive moment $M_r$ is given by

$$M_r = b\left(F_{y3} + F_{y4}\right) - a\left(F_{y1} + F_{y2}\right) + t\left[\left(R_{x1} + R_{x4}\right) - \left(R_{x2} + R_{x3}\right)\right.$$
$$= \mu \frac{abmg}{a+b}\left[\mathrm{sgn}(\dot{y}_3) - \mathrm{sgn}(\dot{y}_1)\right] + f_r \frac{tmg}{2}\left[\mathrm{sgn}(\dot{x}_1) - \mathrm{sgn}(\dot{x}_2)\right]$$

Thus the terms $M_r$, $F_y$, and $R_x$ are defined in terms of state variables $\dot{x}$, $\dot{y}$, and $\dot{\theta}$. From this, we can set up a set of first order linear equations.

# CHAPTER 3

# SOLID MODELING AND SIMULATION OF ATRV-JR

This section presents simulated and experimental results to demonstrate skid steered robot motion. Simulation results are presented first using the friction model. Then the experimental procedure and results are presented and compared with the simulation results.

## 3.1 CAD Modeling

A CAD model of the ATRV-Jr. is developed using Pro-E. Only those parts are modeled which have significant effect on skid steering dynamics such as motor, wheel, tire, base frame, battery etc. Figure 3.1 shows the CAD model of ATRV-Jr. This model is useful to

1) Perform dynamic simulation in ADAMS
2) Examine performance under various road conditions and ground tire interactions
3) Determine angle of tip over without experiment
4) Determine conditions where the robot performs well and safely

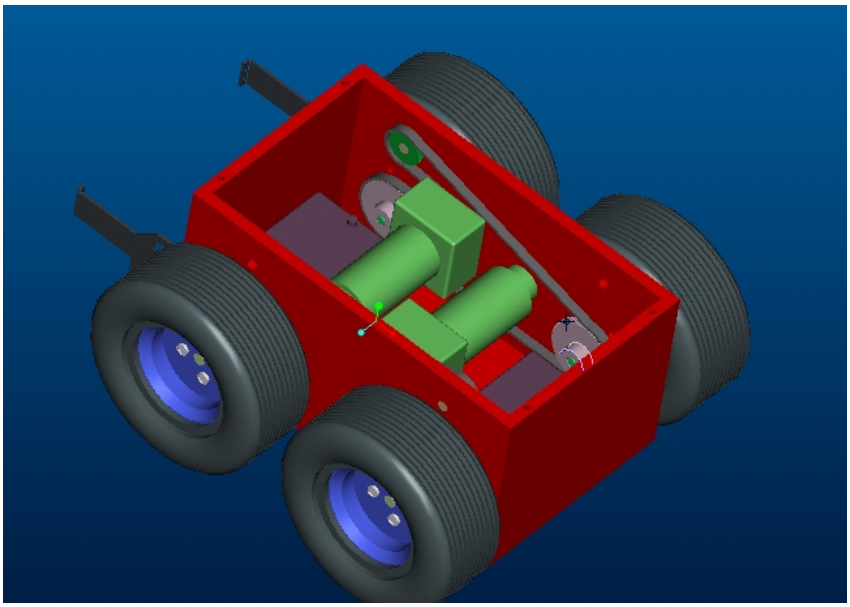

Figure 3.1-1 CAD Model of ATRV-Jr.

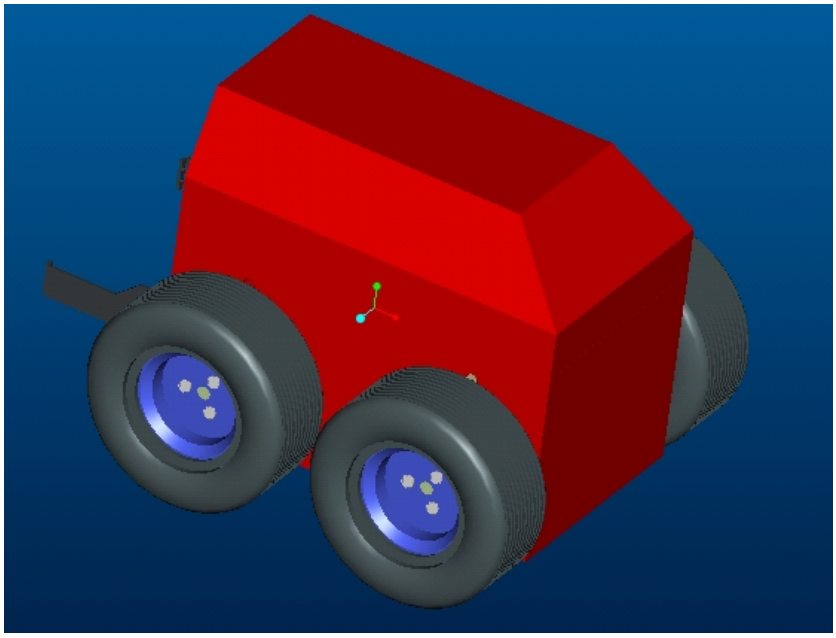

Figure 3.1-2 CAD Model of ATRV-Jr assembly

### 3.2 Matlab Simulation and Results

The three-degree-of-freedom vehicle model's equations of motion must be rewritten in first order differential equation form to enable using first-order numerical integration methods, such as the third order Runge-Kutta, which was used in this study. Inputs into the vehicle are torques provided by LHS and RHS side servomotors. The third order Runge-Kutta integration routine is used to integrate vehicle equations of motion. The Matlab command **ode45** is used to solve simultaneous first order differential equations. The state space representation of dynamic equations (2) is

$$X_1 = \dot{\theta}$$

$$X_2 = \dot{x}$$

$$X_3 = \dot{y}$$

$$X_4 = X$$

$$X_5 = Y$$

$$X_6 = \theta$$

$$\dot{X}_1 = \frac{2t\left(F_{x1} - F_{x2}\right) - M_r}{I}$$

$$\dot{X}_2 = \frac{\left(F_{x1} + F_{x2}\right) - R_x}{m} + X_3 X_1$$

$$\dot{X}_3 = -\frac{F_y}{m} - X_2 X_1$$

$$\dot{X}_4 = X_3 \sin X_6 + X_2 \cos X_6$$

$$\dot{X}_5 = X_3 \cos X_6 - X_2 \sin X_6$$

$$\dot{X}_6 = X_1$$

Let $r$ = wheel radius. Then the input torques supplied by the motors are $\tau_1 = 2rF_{x1}$ and $\tau_2 = 2rF_{x2}$. The above equations can be solved in Matlab using the command ode45. Vehicle parameters (approximate) used for simulation are:

$a$ = 0.37 m, $b$ = 0.55 m, $2t$ = 0.63 m, $r$ = 0.2, $m$ = 116 kg, $I$ = 20 kgm$^2$

1) If the input torques to both motors are same, then the robot should travel along a straight path as shown in the plot of $Y$ vs. $X$ (figure 3.2)

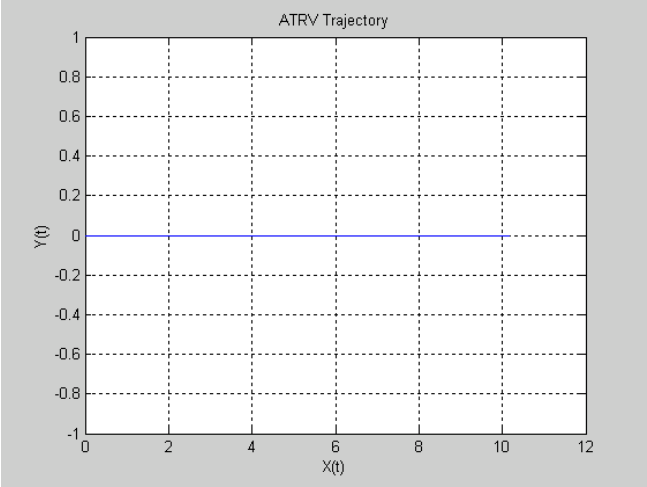


Figure 3.2 ATRV-Jr Trajectory for case 1

2) If the torques to both motors are the same but opposite in direction, then the robot follows the motion as shown in Figure 3.3

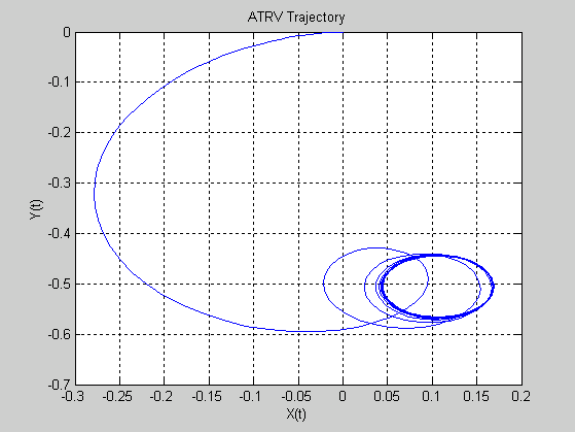


Figure 3.3 Trajectory of robot for case 2

The robot keeps rotating in progressively smaller ovals. The longitudinal and lateral velocities are shown in Figure 3.4. The lateral force (Figure 3.5) becomes constant after some time.

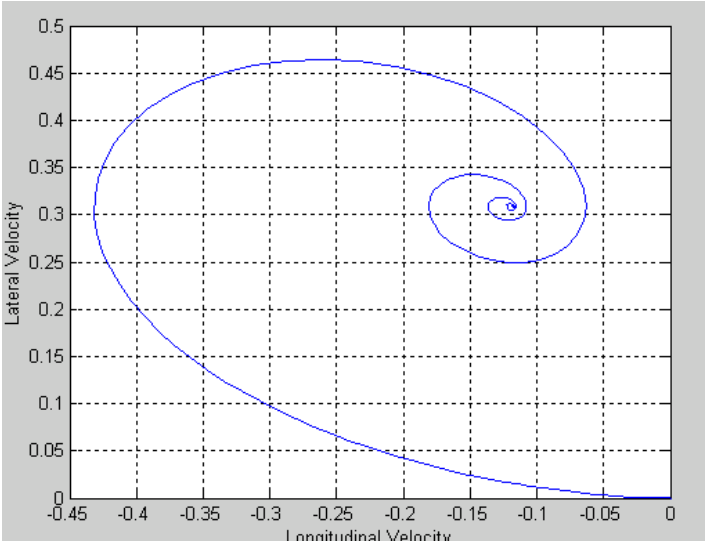

Figure 3.4 Lateral Velocity vs Longitudinal Velocity

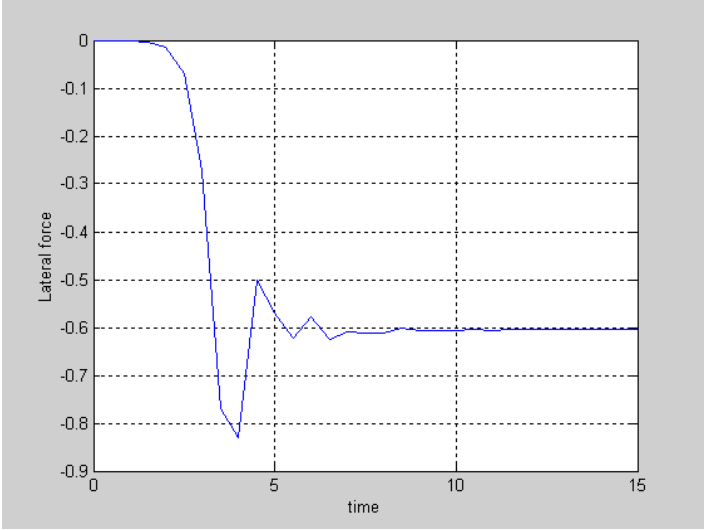

Figure 3.5 Lateral force vs time

Figure 3.6 shows that angular acceleration increases with time and remains at steady state value after some time. This is due to the fact that torque difference between motors increases with time and comes to steady state value after some time.

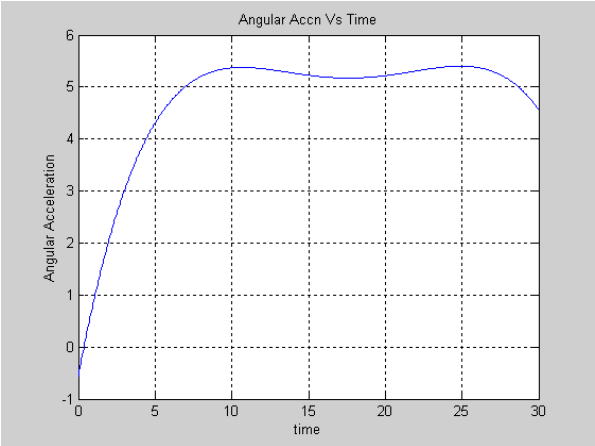


Figure 3.6 Angular Acceleration vs time

Figures 3.7, 3.8, 3.9 show the variation in Vx and Vy. Due to equal and opposite torques at the motors, Vx varies as a sin function of time with progressively reducing amplitude. Vy (lateral skidding) keeps on increasing as the torque from both motors increases in opposite directions.

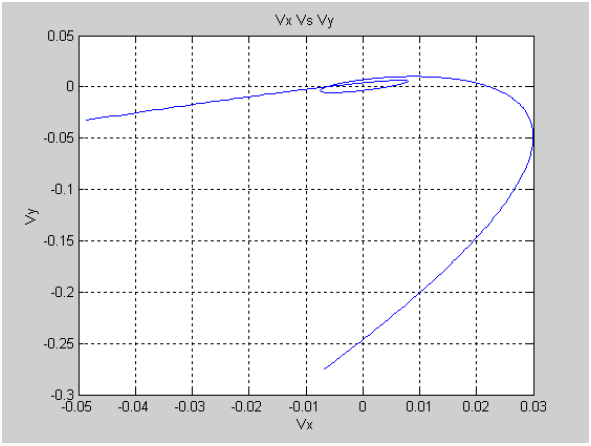


Figure 3.7 Vx vs Vy

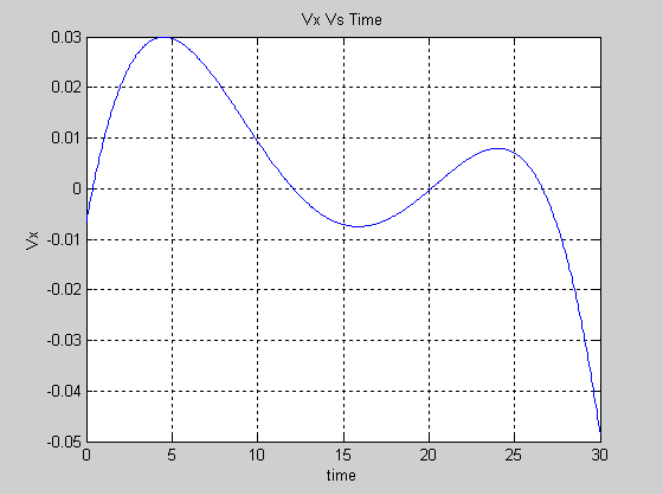


Fig 3.8 Vx vs time

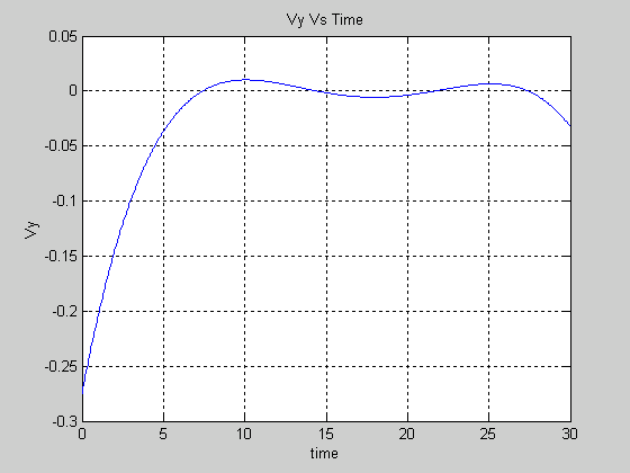


Figure 3.9 Vy vs time

### 3.3 ADAMS Model and Simulation

The solid model was also transferred to ADAMS. To represent the motor to wheel connection as in the actual robot, a coupler was used with same gear ratio. This allows torque to be used as the input to the motors on each side during simulation. (We have

used torque as input in Matlab simulation). Also, inertia associated with the motor, belt, and gear can be modeled in the coupler.

The road surface attached to the tire can be modeled to simulate real life terrain conditions using a coefficient of static friction and kinematic friction, and cohesion and pressure angle to include soil mechanics. Also the user can define the mass and inertia of system and its location.

The following three simulations were performed

1) Using the same input torque on each side of robot
2) Equal and opposite torque on either side of robot
3) A robot motion simulation traveling on road with bumps

**For equal and opposite input** (Figures 3.10, 3.11, 3.12, 3.13)

Figure 3.10 shows trajectory of robot when equal and opposite torques are applied at the motors.

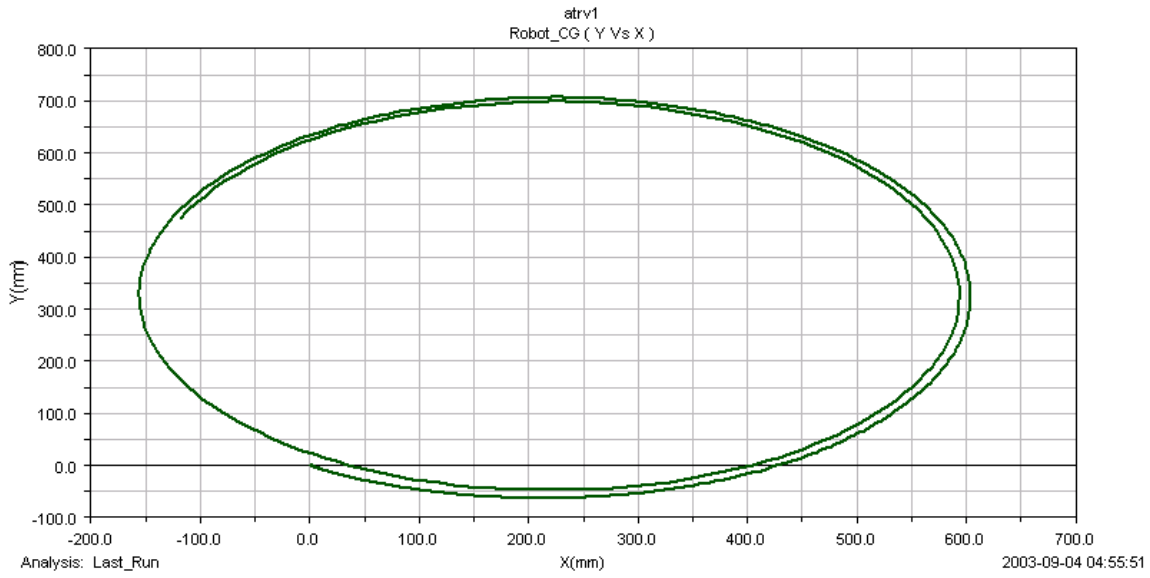


Figure 3.10 Y vs X

Figure 3.11 shows Vy vs Vx. As the torques from motors are equal and opposite, the phase plane trajectory is an increasing spiral pattern.

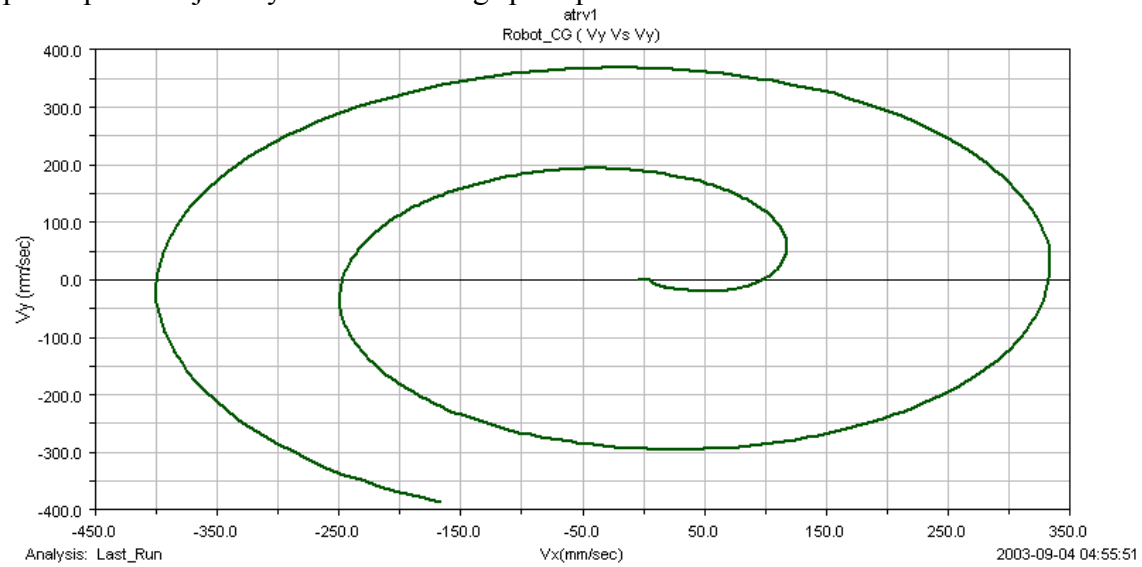


Figure 3.11 Vy Vs Vx

In Figure 3.12, we see that angular velocity of robot increases with time due to the fact that torques are equal and opposite which gives constant angular acceleration.

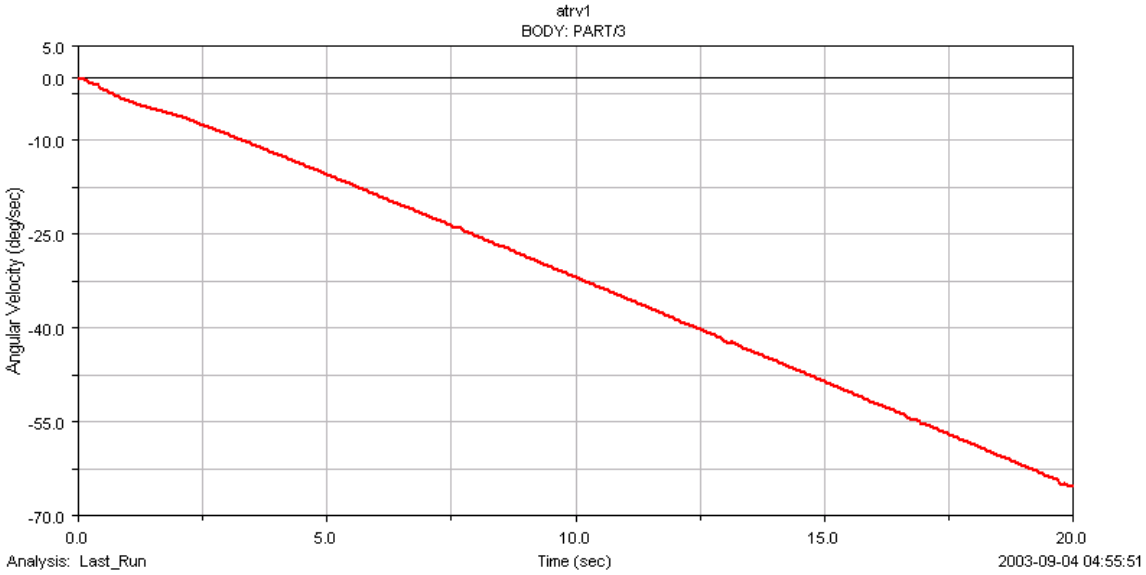


Figure 3.12 Angular Velocity Vs time

Figure 3.13 shows the slip at each tire with time. From the plot, it can be verified that skid steering requires a very high degree of slip at each tire and hence power consumption is also high.

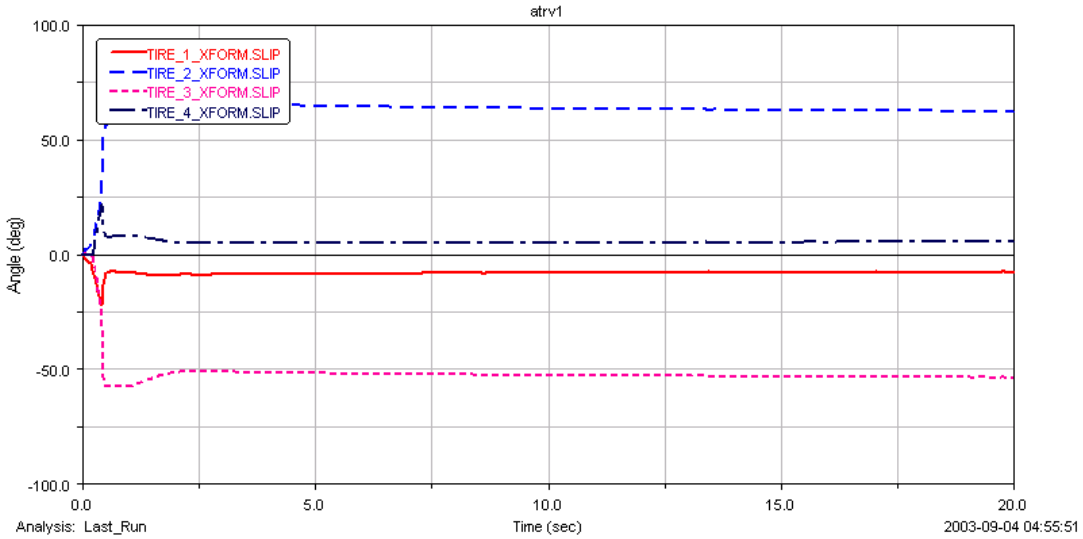


Figure 3.13 Tire slip Vs time

**3.4 Simulation on road with bumps** (Figures 3.14, 3.15)

Figure 3.14 shows *z* acceleration variation with time. As the robot comes across the bump, we see some oscillations as this robot doesn't have any suspension. The stability of the robot is decided by its velocity and the bump dimensions.

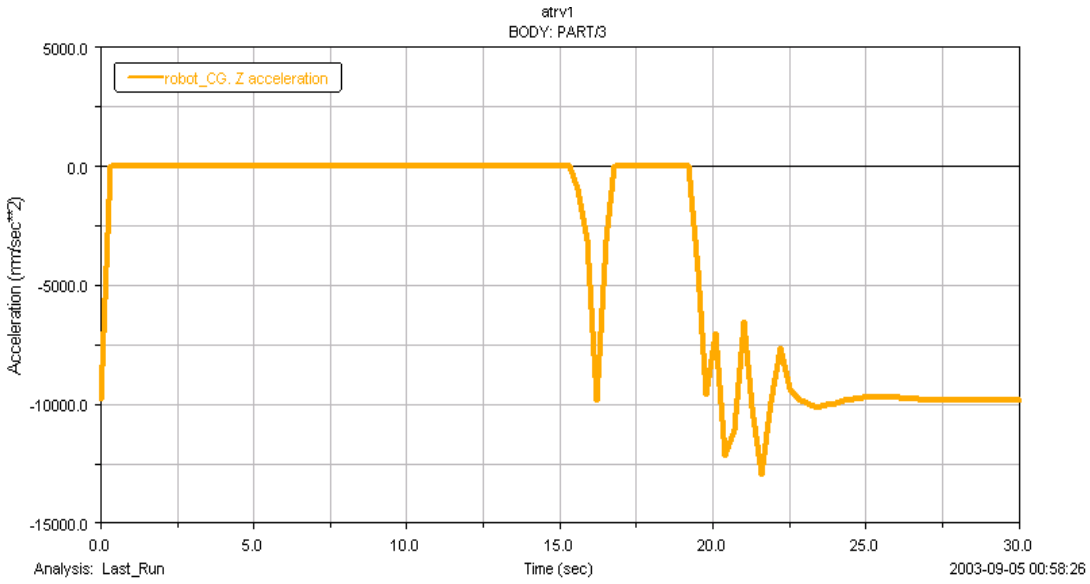


Figure 3.14 Acceleration (*z*) vs time

Figure 3.15 shows the roll and pitch motion of robot when it comes across a bump on road.

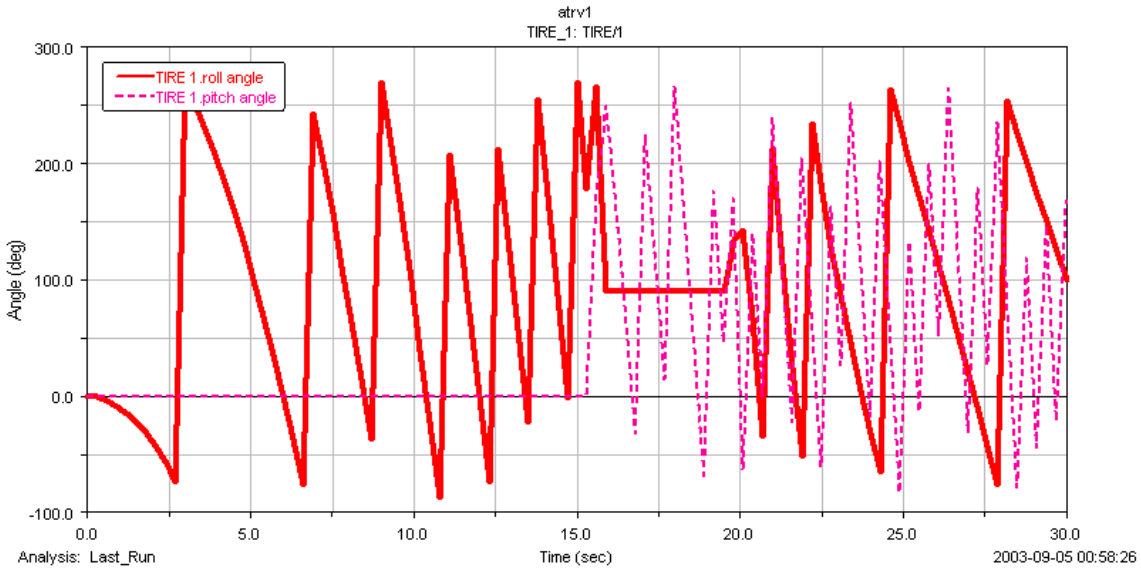


Figure 3.15 Roll and pitch angle vs time

### 3.5 Conclusion

From the ADAMS simulations and Matlab simulations, it can be seen that they don't match exactly but they are similar in nature. This is due in part to the fact that the ADAMS tire model uses a much more complex model for the calculation of lateral and longitudinal resistance, slip etc. Also from the dynamic analysis, it can be seen that tire slip is very high. In the plot of Figure 3.14, the spikes correspond to the bump on the road. Thus robot dynamics are able to identify bumps on the road and from the plot, we might be able to determine the type of terrain.

# CHAPTER 4

# CONCEPT DESIGN OF 4 WHEEL STEERING

While going through the research literature [10], the following concepts were found useful and can be applied to the XUV. These concepts are already implemented on similar robots at Carnegie Mellon University.

## 4.1 Concept 1: Articulated Axle

A passively articulated axle steering can be used for the XUV. It can be implemented by adding a free pivot to one of the vehicle axles. This type of steering is common in wagons and carts. One disadvantage of single axle steering is that the wheels run in separate tracks when going around curves. The advantages include mechanical simplicity, relatively low steering power and moderate maneuverability. This type of design is used in Hyperion in which the velocity of the front wheels is electronically controlled to maintain a desired angle of the front axle.

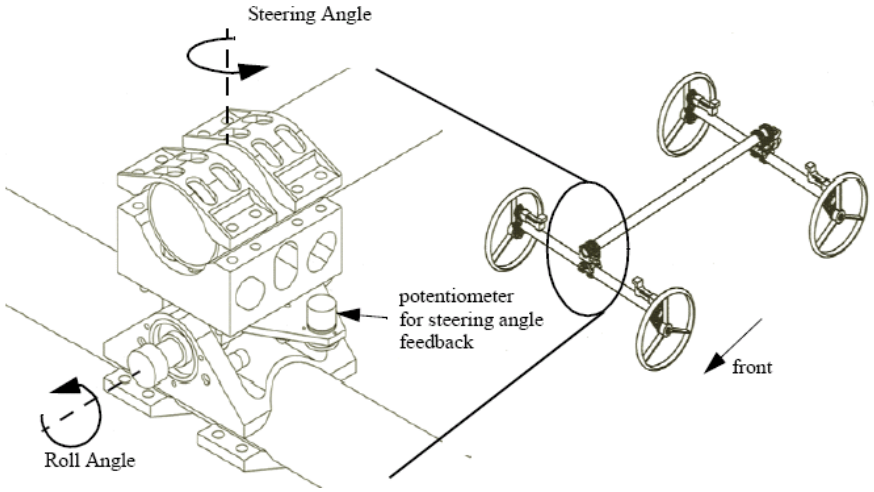


Figure 4.1 Hyperion Rover ([10], Robot used for Mars Excavation)

$$\omega_{front} = f(v_d, \theta_d)$$

$$\omega_{rear} = f(v_d, \theta_a)$$

$$\Delta\omega = K_p(\theta_d - \theta_a)$$

The passively articulated steering joint is composed of two free rotations. The first is about the vertical axis which allows the change in heading of the front axle. The second rotation allows a roll motion of the front axle which is necessary to enable all four wheels to contact the ground over rough terrain. Each wheel is separately driven by a DC motor.

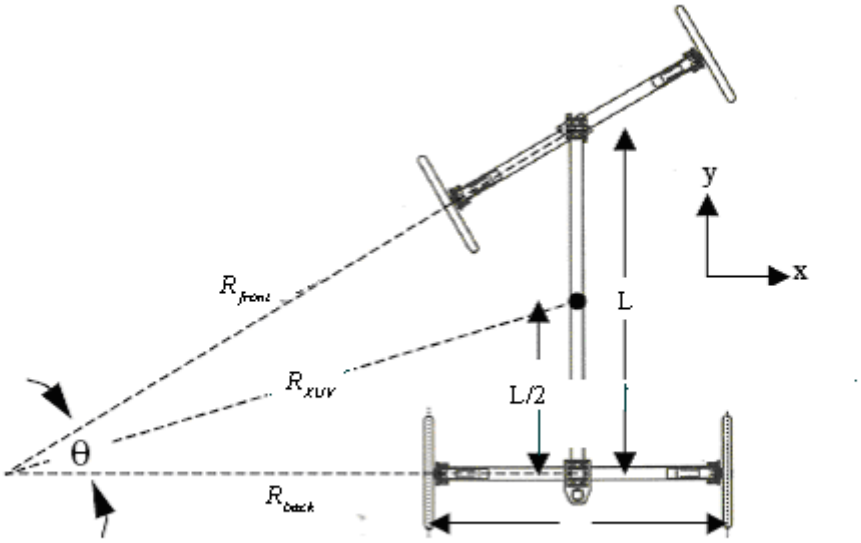


Figure 4.2 Steering geometry

Kinematic Model

The desired velocity and desired angle are those of the center of gravity. Using geometry

$$R_{XUV} = \frac{L}{2\sin\theta}$$

$$R_{XUV} = \sqrt{R_{back}(\theta)^2 + \left(\frac{L}{2}\right)^2}$$

$$R_{back} = \sqrt{R_{front}(\theta)^2 - L^2}$$

The angular velocities are given by

$$\omega_{innerfront} = \frac{v_d}{2\pi r_{wheel}} \frac{R_{front}(\theta_d) - \frac{B}{2}}{R_{XUV}(\theta_d)}$$

$$\omega_{outerfront} = \frac{v_d}{2\pi r_{wheel}} \frac{R_{front}(\theta_d) + \frac{B}{2}}{R_{XUV}(\theta_d)}$$

$$\omega_{innerrear} = \frac{v_d}{2\pi r_{wheel}} \frac{R_{back}(\theta_a) - \frac{B}{2}}{R_{XUV}(\theta_a)}$$

$$\omega_{outerrear} = \frac{v_d}{2\pi r_{wheel}} \frac{R_{back}(\theta_a) + \frac{B}{2}}{R_{XUV}(\theta_a)}$$

The $\{\theta_d, v_d\}$ mobility commands must be translated into angular velocities of each of the four wheels. This calculation is performed using a kinematic model which consists of the seven equations shown above. Note that the front wheel angular velocities are based on the desired steering axle angle, $\theta_d$. In contrast, the rear wheel velocities are based on the current actual steering axle angle, $\theta_a$. If the rear wheels, which are attached to a non-pivoting axle, do not spin at a rate based on the actual steering axle angle, the chassis undergoes excessive stresses and disturbs the velocity control of the wheel motors. Because the front axle can freely pivot, the front wheels can spin at a rate based on the desired steering axle angle, which forces the axle to the proper angle.

Simply commanding the front wheel velocities based on desired steering axle angle does pivot the axle. A proportional controller can be added. The output of this controller is subtracted from the front inner wheel and added to the front outer wheel. The output is based on the difference between the desired and actual steering axle angle.

### 4.2 Concept 2 : Vehicle speed sensing type four wheel steering (4WS)

In this method , the steering angle of the rear wheels changes according to the vehicle's speed. The system works in three principle phases — negative, neutral, and positive. At low speeds, the rear wheels turn in a direction opposite to the front wheels (negative phase). At high speeds, the rear wheels turn in the same direction as the front wheels (positive phase). At moderate speeds the rear wheels remain straight (neutral phase).

The XUV has an independent suspension model. In this model, instead of a steering mechanism, a speed sensor and controller are needed at the rear wheels. This method was researched by Sano et al [1]. The steering equation between the front and rear wheels can be obtained from following equation:

$$K_s = \frac{\delta_r}{\delta_f} = \frac{\frac{Ma}{C_r L} U_x{}^2 - b}{\frac{Mb}{C_f L} U_x{}^2 + a}$$

where all the terms have meaning

$U_x =$ longitudinal Velocity

$U_y =$ lateral velocity

$C_f =$ front tire cornering stiffness

$C_r =$ rear tire cornering stiffness

$\delta_f =$ front steering angle

$\delta_r =$ rear steering angle

$a =$ front tire distance from CG along longitudinal axis

$b =$ rear tire distance from CG along longitudinal axis

$M =$ mass of vehicle

$L =$ vehicle wheelbase

The characteristic curve is shown in Figure 4.3.

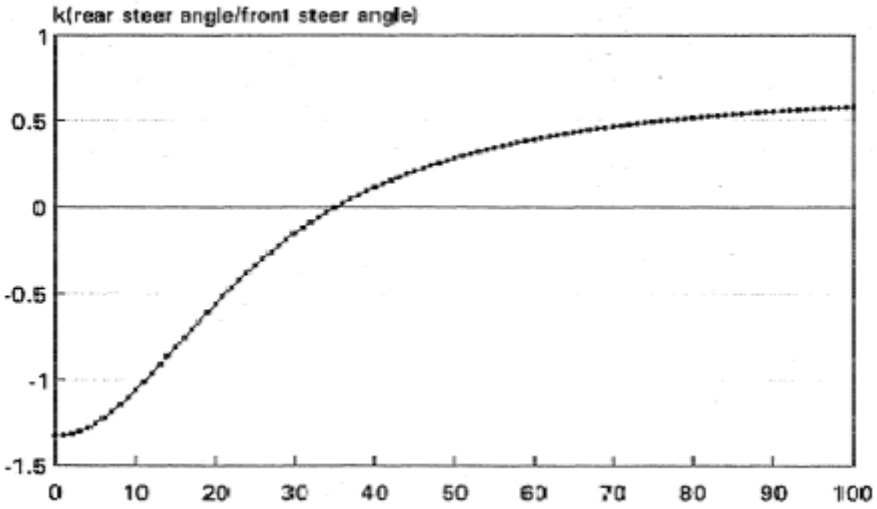


Vehicle speed ( miles/hr )

Figure 4.3 Characteristic Curve

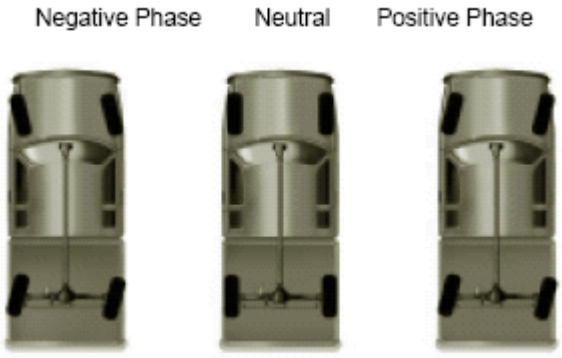


Figure 4.4 Wheel steering phases (Source: Service Tech Magazine Sept 2001)

Figure 4.4 shows a typical four wheel steering vehicle. Both steering systems (front and rear) are parallel. For the XUV, since it's maximum speed is 30 miles/hr, we mainly need rear wheel steering to turn the rear wheels in the opposite direction. This will help to avoid obstacles and in parking maneuvers where speed is very low.

Figure 4.5 shows a typical case, of vehicle making turn. The pivot point lies along the centerline passing through the CG of vehicle. This type of steering is also known as crab steering. Given a desired velocity and turn radius, from the above relation, the angular wheel velocity for each forward velocity can be calculated. This will then require a controller in each wheel which will sense the speed and position of each wheel. It also assumes the steering angle at the rear is equal and opposite to the front steering angle

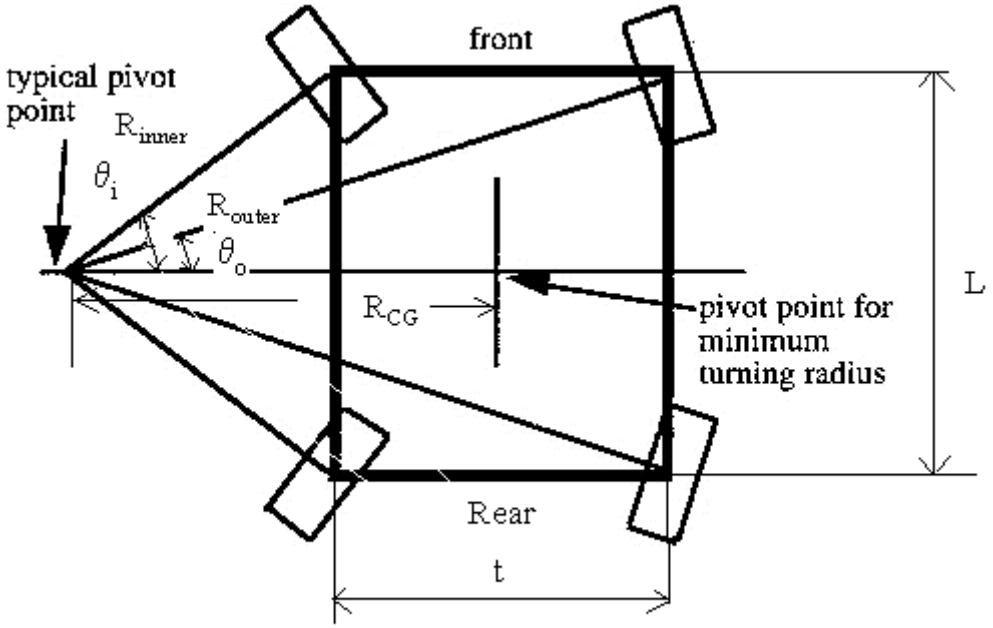


Figure 4.5 Four wheel steering geometry

Assuming $K_s = -1$, where the real wheel steering angle is equal and opposite to the front wheel steering angle, a relation for the angular velocity of each wheel is developed. Referring to Figure 4.5, when the vehicle makes a turn, the inside and outside wheels follow a circular track. A relation between the angle of the inside wheels and the angle of the outside wheels can be derived as follows:

$$\tan\left(\theta_{outer}\right)=\frac{L/2}{x+t}$$

$$\tan\left(\theta_{inner}\right)=\frac{L/2}{x}$$

Then

$$\cot\left(\theta_{outer}\right)=\frac{2x+2t}{L}=\cot\left(\theta_{inner}\right)+\frac{2t}{L}$$

$$\theta_{outer}=\cot^{-1}\left(\cot\left(\theta_{inner}\right)+\frac{2*\text{track length}}{\text{wheelbase}}\right.$$

From the geometry

$$R_{\text{inner}}=\frac{R_{CG}-\frac{t}{2}}{\cos\left(\theta_i\right)}$$

$$R_{\text{outer}}=\frac{R_{CG}+\frac{t}{2}}{\cos\left(\theta_o\right)}$$

$$\omega_{\text{rear inner}}=\omega_{\text{front inner}}=\frac{v_d}{2\pi r_{\text{wheel}}}\frac{R_{CG}-\frac{t}{2}}{R_{CG}}$$

$$\omega_{\text{rear outer}}=\omega_{\text{front outer}}=\frac{v_d}{2\pi r_{\text{wheel}}}\frac{R_{CG}+\frac{t}{2}}{R_{CG}}$$

# CHAPTER 5

## STEERING SYSTEM MODELING

Exact modeling of the steering system involves mechanical and electrical components as shown in figure 5.1. It is natural that the inertial system consists of the steering wheel and the motor and the spring system is made of the torsion bar and the tire.

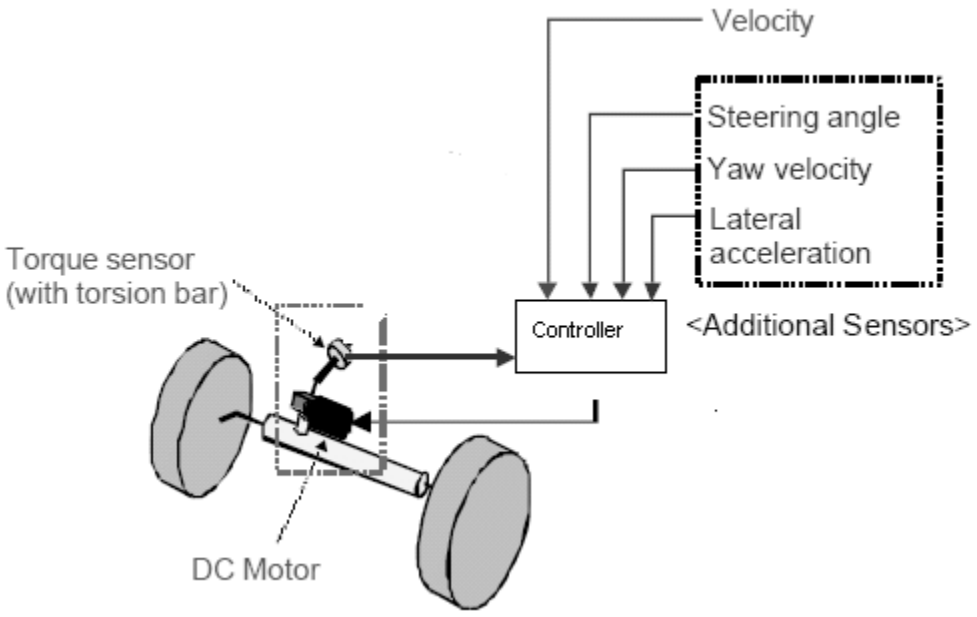


Figure 5.1 Steering system representation

### 5.1 DC Motor Modeling

We have the relation between the steering angular acceleration and the applied torque. The applied torque is generated by the motor. In this, the relation between applied voltage and generated torque can be derived using Kirchoff's voltage law.

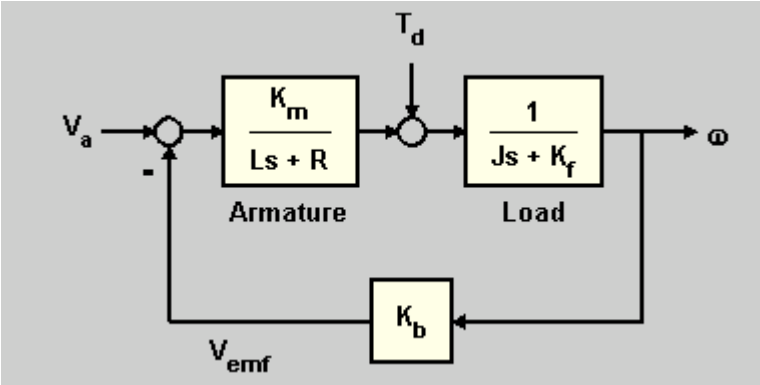


Figure 5.2 DC Motor model

From figure 5.2, the relation between applied voltage and angular velocity of the motor can be derived. Torque supplied by motor will be $T_m = I\dot{\omega}$

$$(V_a - K_b\omega)\left(\frac{K_m}{R\left(s+\frac{L}{R}\right)}\right)\left(\frac{1}{J\left(s+\frac{K_f}{J}\right)}\right) = \omega$$

$$V_a\left(\frac{K_m}{R\left(s+\frac{L}{R}\right)}\right)\left(\frac{1}{J\left(s+\frac{K_f}{J}\right)}\right) = \omega\left(1+\frac{K_bK_m}{RJ\left(s+\frac{L}{R}\right)\left(s+\frac{K_f}{J}\right)}\right)$$

$$\frac{\omega}{V_a} = \frac{d_1}{s^2 + a_1 s + a_2}$$

where

$$d_1 = \frac{K_m}{RJ}$$

$$a_1 = \frac{L}{R} + \frac{K_f}{J}$$

$$a_2 = \frac{L}{R}\frac{K_f}{J} + K_b d_1$$

Thus we see that the motor system can be represented by a second order system. The relation between applied voltage and steering angle can be derived as shown below.

Consider the steering system at the front wheel as shown in Figure 5.3. Around the king pin, the equations describing the steering system are

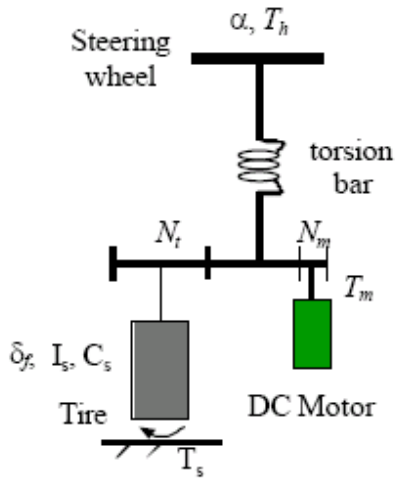


Figure 5.3 Steering system dynamics

$$I_s\ddot{\delta}_f + C_s\dot{\delta}_f + T_s = N_t N_m T_m + N_t T_h$$

Since the XUV is unmanned, $T_h = 0$.

$T_s$ is the self aligning torque

$$T_s = 2\xi C_f\left(\frac{U_y}{U_x} + \frac{ar}{U_x} - \delta_f\right.$$

Putting this into the differential equation for steering

$$I_s\ddot{\delta}_f + C_s\dot{\delta}_f - 2\xi C_f\delta_f + 2\xi C_f\left(\frac{U_y + ar}{U_x}\right. = N_t N_m T_m \tag{3}$$

If we ignore lateral dynamics, we can derive the open loop transfer function for the steering angle to the applied torque

$$I_s\ddot{\delta}_f + C_s\dot{\delta}_f - 2\xi C_f\delta_f = N_t N_m I\dot{\omega}$$

Taking the Laplace transform on both sides

$$s^2 I_s\delta_f + C_s s\delta_f - 2\xi C_f\delta_f = N_t N_m Is\omega$$

Let

$$C_0 = \frac{I_s}{N_t N_m I}$$

$$C_1 = \frac{C_s}{N_t N_m I}$$

$$C_2 = \frac{-2\xi C_f}{N_t N_m I}$$

Then

$$\frac{\delta_f}{\omega} = \frac{s}{C_0 s^2 + C_1 s + C_2}$$

From the relation developed between input voltage and angular velocity

$$\frac{\omega}{V_a} = \frac{d_1}{s^2 + a_1 s + a_2}$$

We can write

$$\frac{\delta_f}{V_a} = \frac{s}{\left(C_0 s^2 + C_1 s + C_2\right)}\frac{d_1}{\left(s^2 + a_1 s + a_2\right)}$$

We see that transfer function between input voltage and steering angle is a third order system.

### 5.2 Steering System Response

In this section, the steering system open loop response is discussed. After its analysis, its closed loop response is considered. The open loop transfer function for the applied voltage to the steering angle is given by the equation

$$\frac{\delta_f}{V_a} = \frac{s}{\left(C_0 s^2 + C_1 s + C_2\right)} \frac{d_1}{\left(s^2 + a_1 s + a_2\right)}$$

Figure 5.4 shows the step input response of the system.

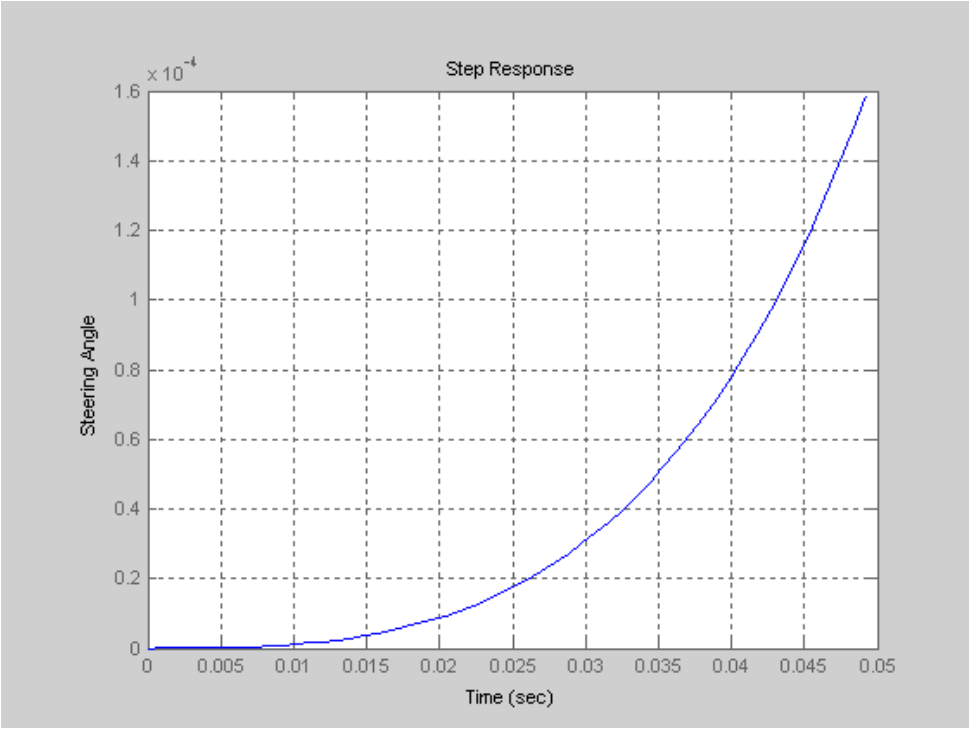


Figure 5.4 Step response of steering system

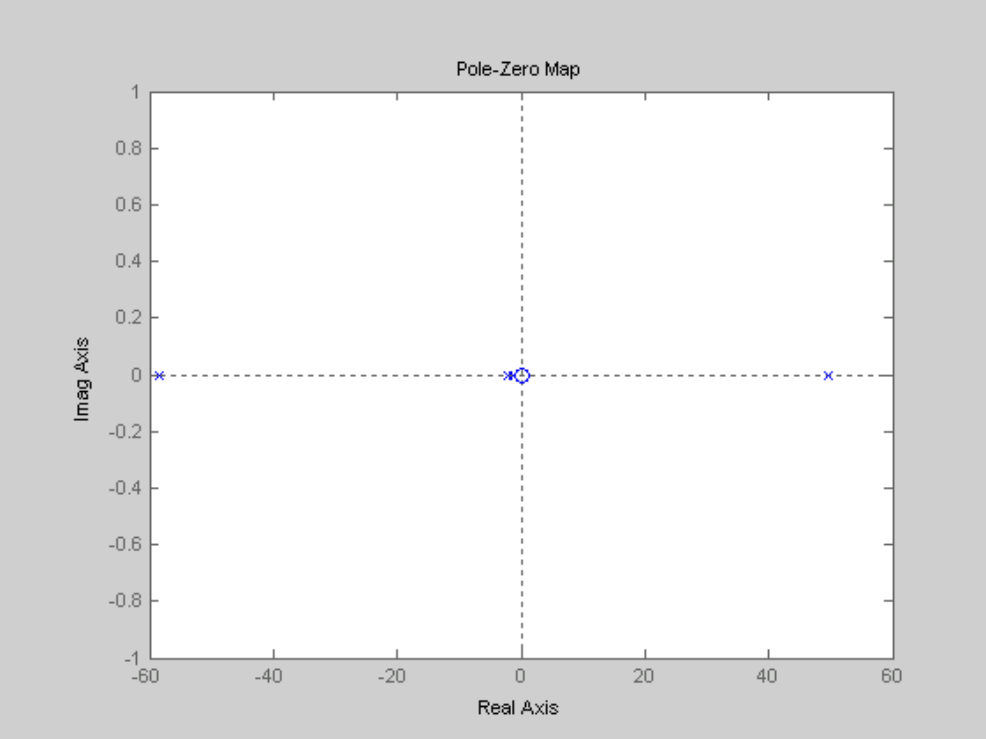

Figure 5.5 Pole – Zero map

The poles of the system are shown in Figure 5.5 and are all real values of (-58.3672), (49.5953), (-2.0537), (-1.3796)

From the pole values above, one pole is in the right half plane which makes the system unstable. To make the system stable and reduce the response time, we can add a PID controller.

# CHAPTER 6

# VEHICLE HANDLING CHARACTERISTICS

A vehicle (XUV) is modeled such that the two front and rear wheels are considered as single front and single rear wheels (bicycle model). The variables of interest are lateral acceleration and yaw rate.

## 6.1 Equations of Motion

The inputs to the system are front wheel steering input and rear wheel steering input.

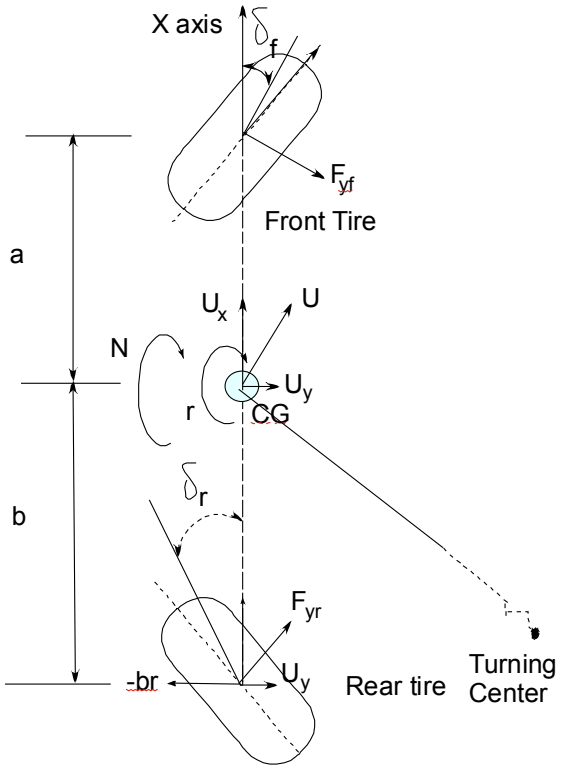


Figure 6.1 Bicycle Model (Free Body Diagram)

The differential equations of motion can be written as

$$ma_y = \quad F_y$$

$$N = I\frac{dr}{dt}$$

$$a_y = U_x r + \dot{U}_y$$

From Figure 6.2, we see that the equations can be written in state space form where the states of the system are the yaw velocity *r* and the lateral acceleration. The inputs to the system are front wheel steering angle and rear wheel steering angle. From Figure 6.2, the slip angles for front and rear can be derived as:

$$\text{tire slip angle for front} = \alpha_F = \frac{v + ar}{V} - \delta_F = \beta + \frac{ar}{V} - \delta_F$$

$$\text{tire slip angle for rear} = \alpha_R = \frac{v - br}{V} + \delta_R = \beta - \frac{br}{V} + \delta_R$$

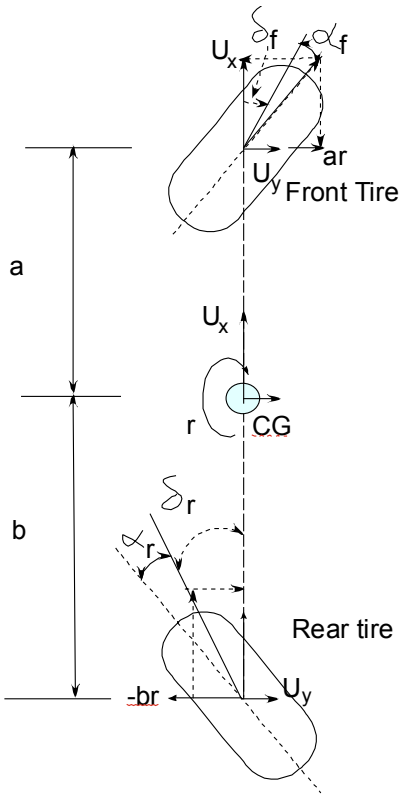


Figure 6.2 Velocities at front and rear tire

The equations of motion can be written as

$$ma_y = F_{yf}\cos\left(\delta_f\right) + F_{yr}\cos\left(\delta_r\right)$$

$$I_z\dot{r} = aF_{yf}\cos\left(\delta_f\right) - bF_{yr}\cos\left(\delta_r\right)$$

$$F_{yf} = C_f\alpha_f = C_f\left(\frac{U_y + ar}{U_x} - \delta_f\right.$$

$$F_{yr} = C_r\alpha_r = C_r\left(\frac{U_y - br}{U_x} + \delta_r\right)$$

**6.2 State Space representation & steering system response**

Making small angle approximations, the equations of motion can be put in state space form

$$X = AX + BU$$

$$Y = CX + DU$$

where $X$ is the state space vector. $U$ is input and $Y$ is output.

$$\begin{bmatrix}\dot{U}_y\\ \dot{r}\end{bmatrix} = \begin{bmatrix}\frac{C_f + C_r}{mU_x} & \frac{aC_f - bC_r}{mU_x}\\ \frac{aC_f - bC_r}{I_zU_x} & \frac{a^2C_f + b^2C_r}{I_zU_x}\end{bmatrix}\begin{bmatrix}U_y\\ r\end{bmatrix} + \begin{bmatrix}-\frac{C_f}{m} & \frac{C_r}{m}\\ \frac{aC_f}{I_z} & \frac{bC_f}{I_z}\end{bmatrix}\begin{bmatrix}\delta_f\\ \delta_r\end{bmatrix}$$

Comparing with the state space form $AX + BU$

$$A = \begin{bmatrix}\frac{C_f + C_r}{mU_x} & \frac{aC_f - bC_r}{mU_x}\\ \frac{aC_f - bC_r}{I_zU_x} & \frac{a^2C_f + b^2C_r}{I_zU_x}\end{bmatrix}$$

$$B = \begin{bmatrix}-\frac{C_f}{m} & \frac{C_r}{m}\\ \frac{aC_f}{I_z} & \frac{bC_f}{I_z}\end{bmatrix}$$

$$X = \begin{bmatrix} U_y \\ r \end{bmatrix}$$

$$U = \begin{bmatrix} \delta_f \\ \delta_r \end{bmatrix}$$

The overall view of the steering system is shown in Figure 6.3.

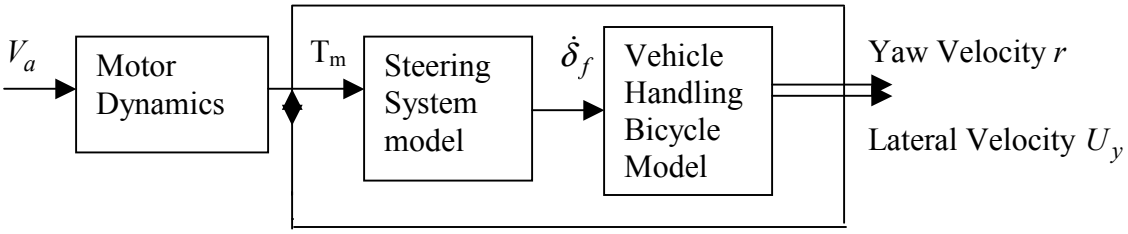


Figure 6.3 Steering system block diagram

The step response of the bicycle model is shown in Figure 6.4.

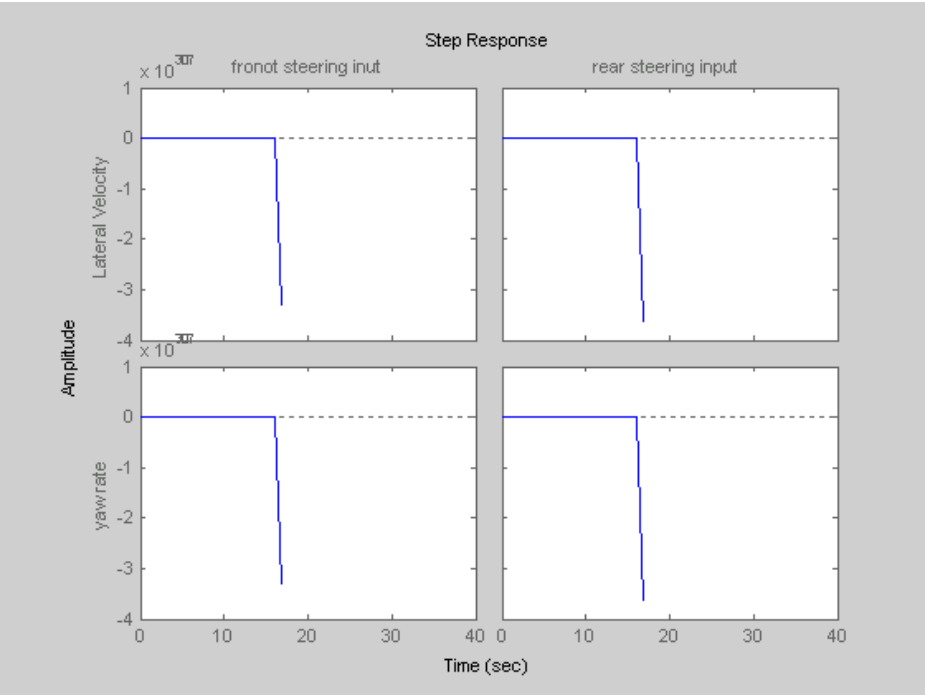


Figure 6.4 Step response of bicycle model

The poles of the system are (33.6328) and (42.3872). Since the poles are in the right half plane, the system is unstable. We can make the system stable by placing poles at (for example) (-10+10i) and (-10-10i). The above points are just generalized points and poles can be placed at any desired location (according to system requirements). The characteristic polynomial for this closed-loop system is the determinant of $\left(sI-\left(A-BK\right)\right)$. Since the matrices $A$ and $B*K$ are both 2 by 2 matrices, there will be 2 poles for the system. By using full-state feedback, we can place the poles anywhere we want. We could use the MATLAB function `place` to find the control matrix $K$ which will give the desired poles. The step response is shown in figure 6.5

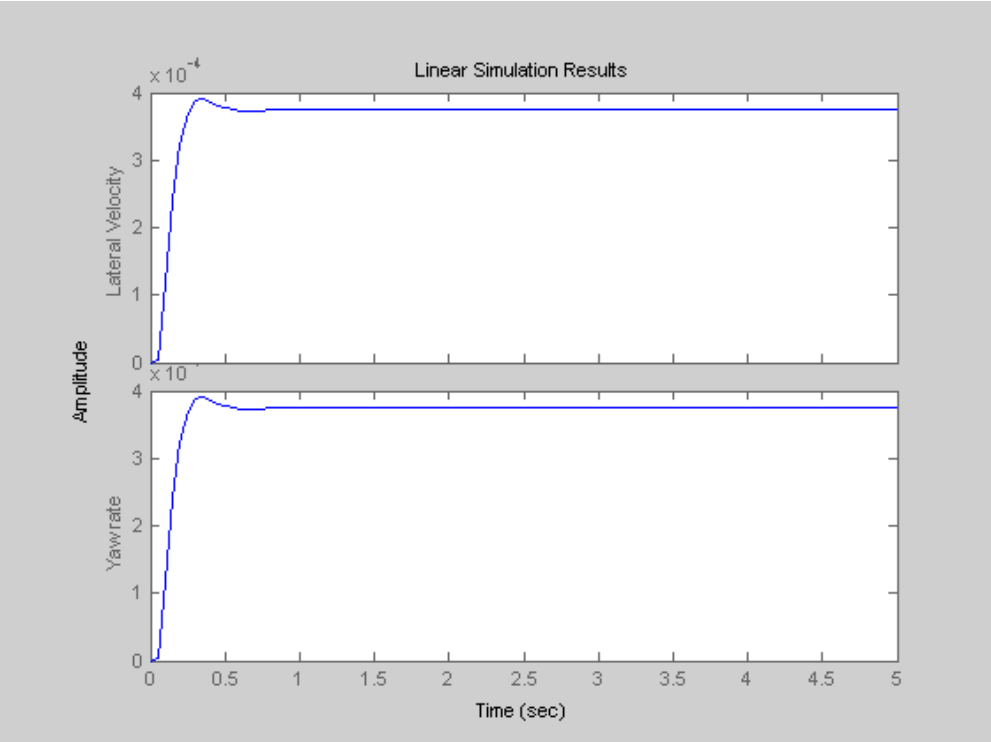


Figure 6.5 Closed loop feedback response

The responses for lateral acceleration and angular acceleration are shown with step input at front and rear in Figures 6.6 and 6.7.

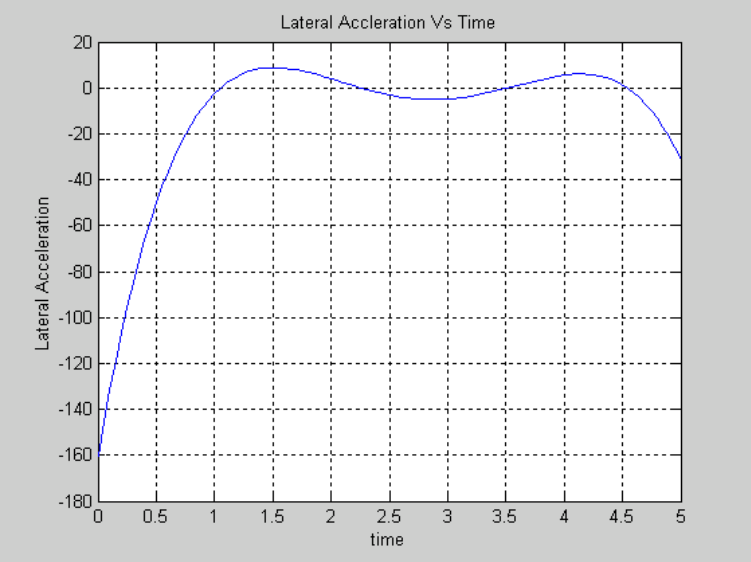


Figure 6.6 Lateral Acceleration vs time

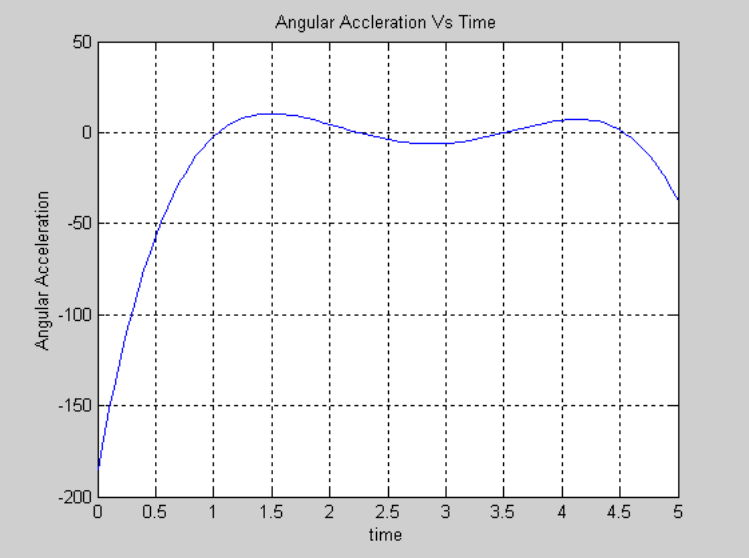


Figure 6.7 Angular acceleration vs time

When both inputs are sinusoidal with phase shifted by 90°, the response of the system is shown in Figures 6.8 to 6.10.

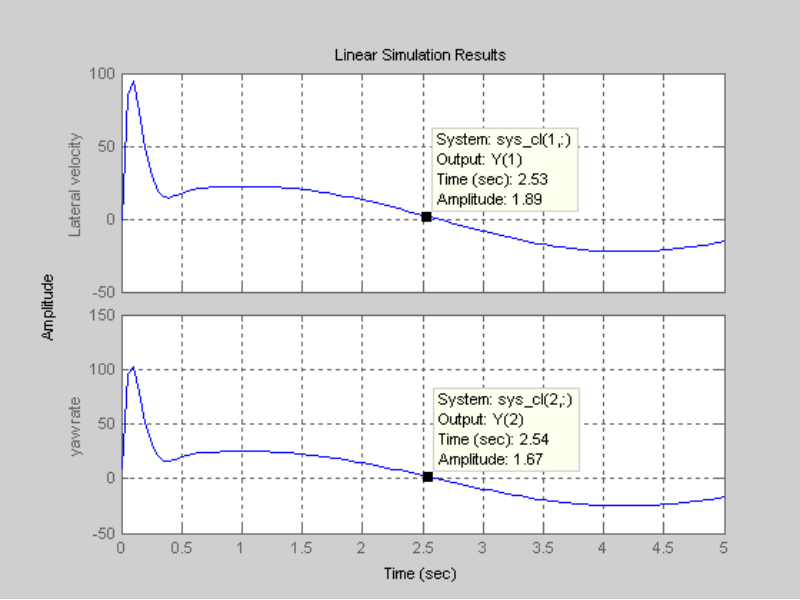

Figure 6.8 Steering system responses for sinusoidal input

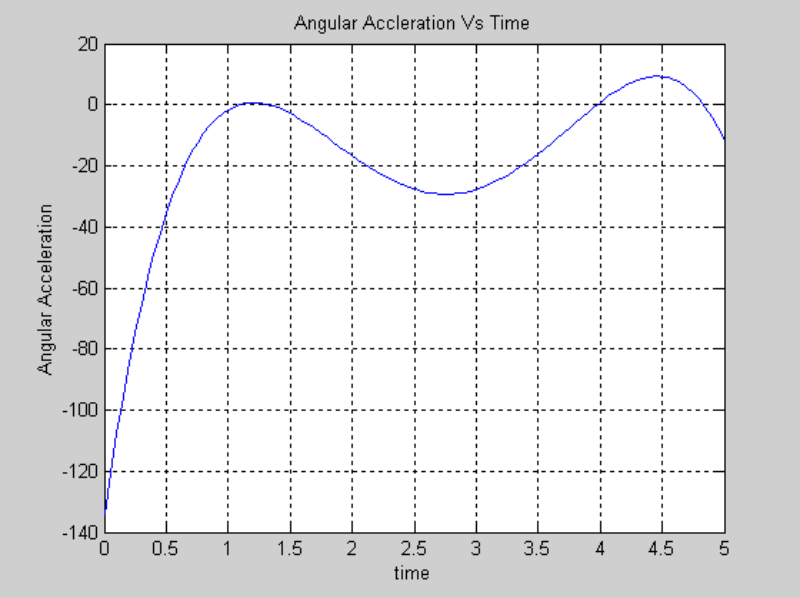

Figure 6.9 Angular acceleration vs time

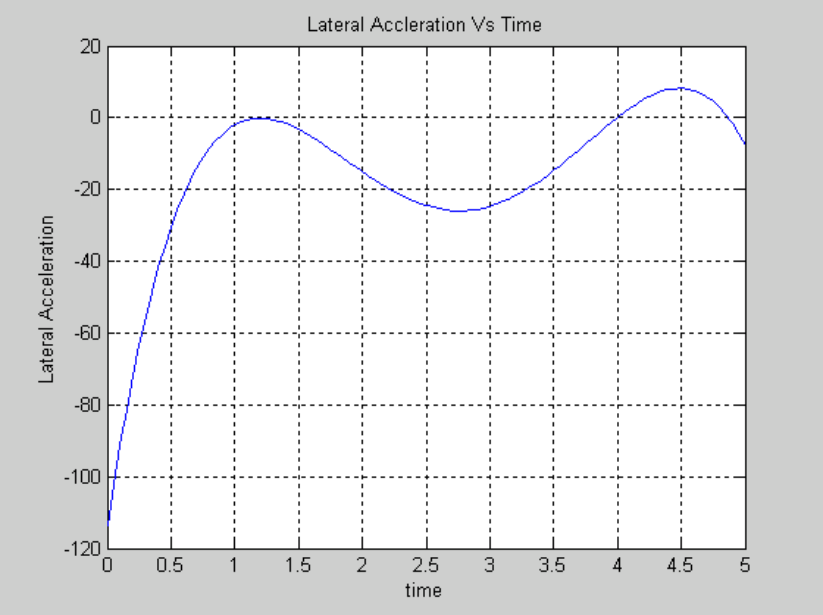

Figure 6.10 Lateral acceleration vs time

From the plots, we see that the behavior of the two states is very similar. This is due to the fact that each state depends on both the inputs and any change in input is distributed equally due to vehicle symmetry conditions. This can be verified from matrices $A$ and $B$ in state space equations,

$$A = \begin{bmatrix} 42.00 & -1.80 \\ -1.80 & 34.02 \end{bmatrix}$$

$$B = \begin{bmatrix} -1.00 & -1.10 \\ -0.90 & -0.99 \end{bmatrix}$$

# CHAPTER 7

# DYNAMIC ANALYSIS OF FOUR WHEEL STEERING

Mobile robots are being developed for applications in rough terrain, such as planetary exploration, mining, hazardous site inspection, and military reconnaissance. In most of these applications, it would be desirable for the robot to have greater maneuverability and a sturdy steering system. Steering systems that are used for robotic vehicles can be similar to those used in automobiles except robotic vehicles are autonomous. The research focus is on the development of reconnaissance vehicles with improved performance, increased stability, and enhanced maneuverability. In this section, an existing technology such as four wheel steering (4WS) is discussed. Recent research on 4WS devices is constantly advancing the technology.

It was observed that little research has been done which examines the important vehicle dynamic aspects. This section mainly focuses on the development and analysis of a dynamical model before considering control aspects of four wheel steering. Such results are presented to make the application of the control system on an actual vehicle easier. This research sets a goal of making data useful for the development of a 4WS device through t computer simulation models and dynamic analyses.

In Chapter 5, the bicycle model for the four wheel steering vehicle was is developed and vehicle handling characteristics were discussed using Matlab simulations. Also a mathematical model relating rear wheel steering input to front wheel steering input was developed. In this section, ADAMS was used to simulate the vehicle model. The 3D vehicle model of the XUV is developed in ADAMS. To validate the model, ADAMS demonstration steering model results are used. The same input shown in Figure 7.2 is given to the XUV model. The results of both models are compared for validation of the XUV model.

The requirements for steering systems are becoming even more diverse. The demand for optimal feedback leads inevitably to the employment of rack-and-pinion steering systems, especially for vehicles with high front axle loads. Because rack-and-pinion steering typically shows a significantly higher efficiency from the tie rod to the steering shaft the desired feedback can be achieved. Figure 7.4 shows the XUV ADAMS model.

A common rack-and-pinion arrangement is used for front steering. The pinion is driven by a motor (not shown in model). As discussed earlier, rear wheel steering input will be a function of input steering. The ratio of rear wheel steering to front wheel steering used here is -1. This is used since the maximum speed of XUV is 40 miles/hr which falls under the low speed category. Referring to Figure 7.9, at low speeds, the rear wheels will move opposite to the front wheels, which gives greater maneuverability for the vehicle. As the speed increases, the ratio $K_s$ also changes accordingly and the rear wheel moves accordingly. The results in this section are discussed for $K_s = -1$.

### 7.1 ADAMS demonstration steering model

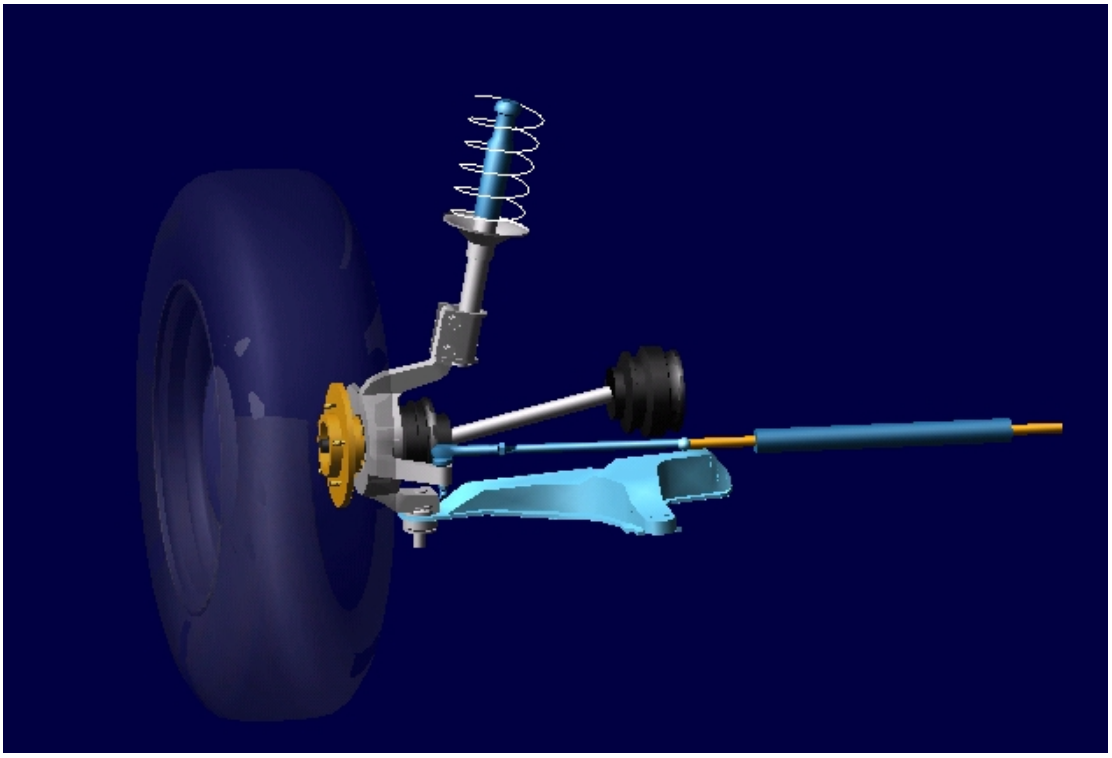

Figure 7.1 Steering demonstration model in ADAMS

The input to the rack is given as shown in Figure 7.2

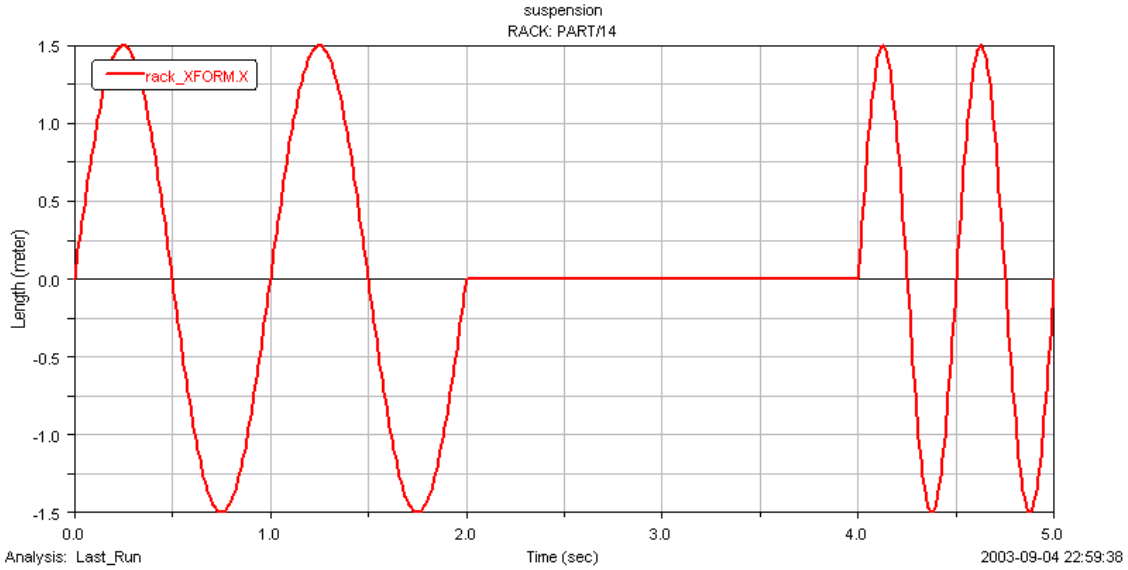


Figure 7.2 rack input

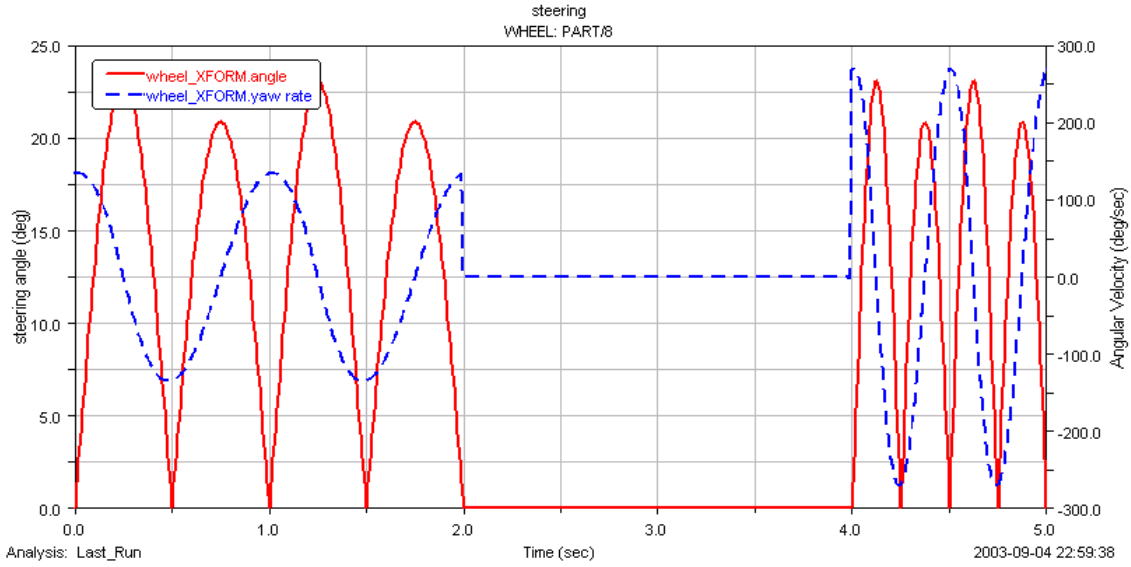


Figure 7.3-Wheel response (yaw rate and steering angle)

As seen from Figure 7.3, the steering angle follows the steering input. The angular velocity also follows the input.

### 7.2 XUV four wheel steering model response

The four wheel steering model developed for the XUV is shown in figure 7.4. The sphere shown in the model represents the mass and inertia of XUV (2000 kg).
The front wheel steering input is shown in Figure 7.5.

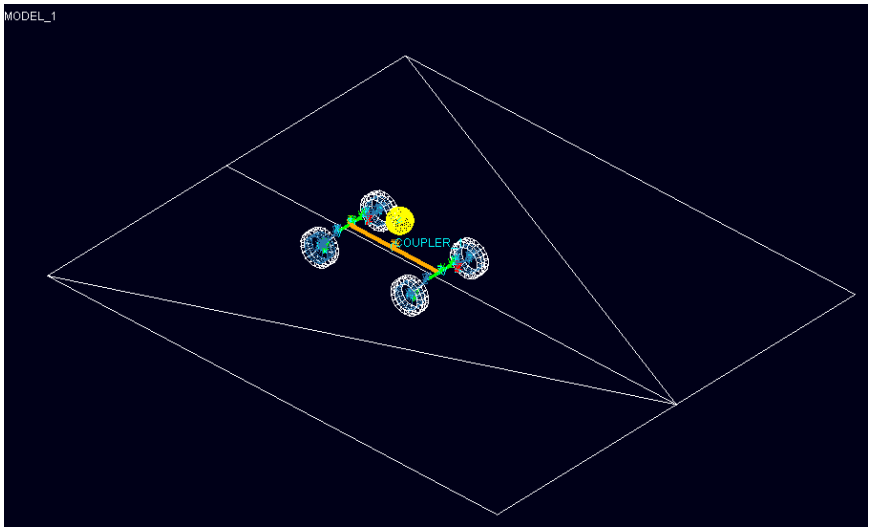

Figure 7.4 XUV model of 4WS

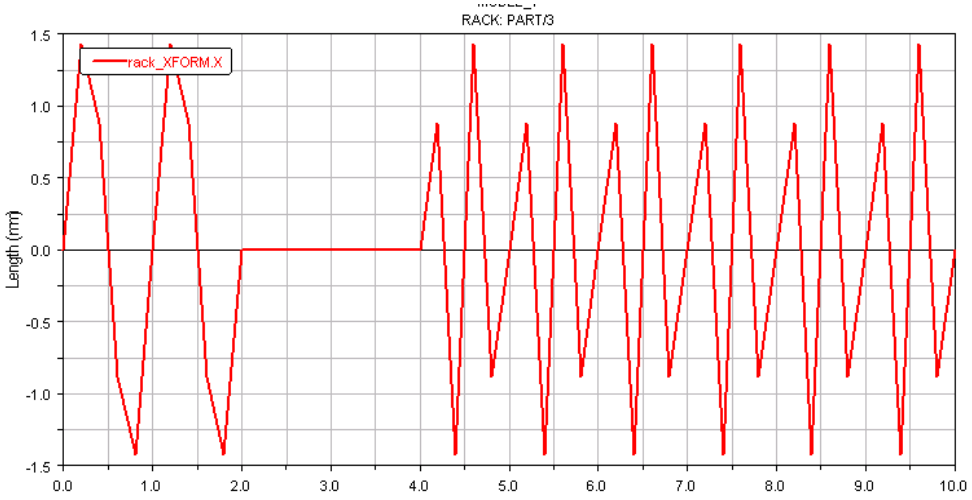

Figure 7.5 Rack displacement

The corresponding left wheel yaw rate is shown below in Figure 7.6. From the plot, it can be seen that yaw rate also follows the input.

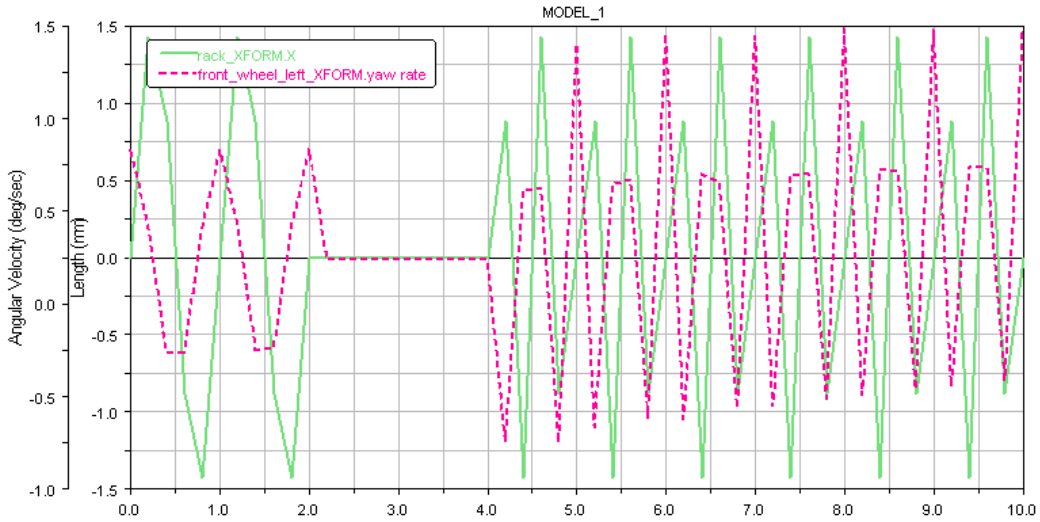


Figure 7.6 Rack displacement and yaw rate comparison

By comparing the responses of the demonstration model and XUV model, it can be seen that results are similar. This shows that joints used for the rack-and-pinion mechanism are correct for the XUV model. Different types of front steering inputs were given and simulation results are shown below.

1) $K_s = -1$, step input to front steering (30 mm displacement in 4 seconds)

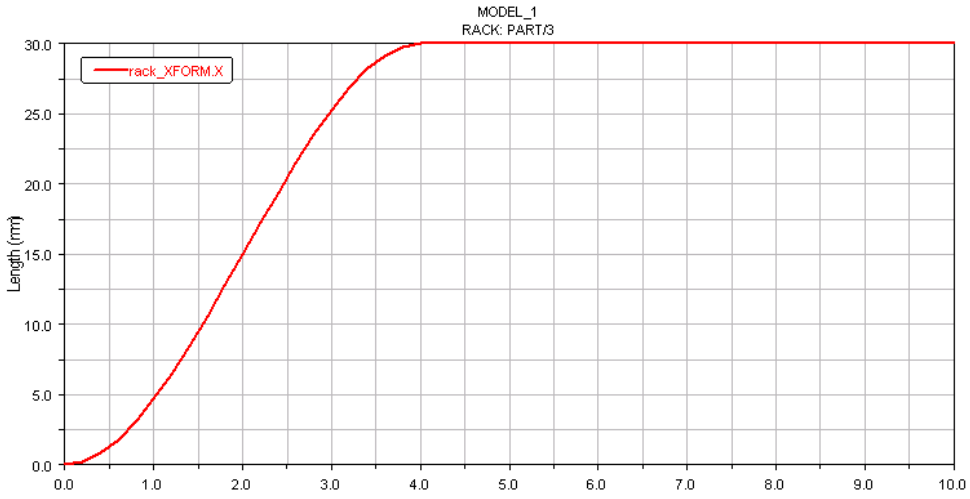


Figure 7.7 Rack displacement

The front and rear steering angles are compared in Figures 7.8 and 7.9.

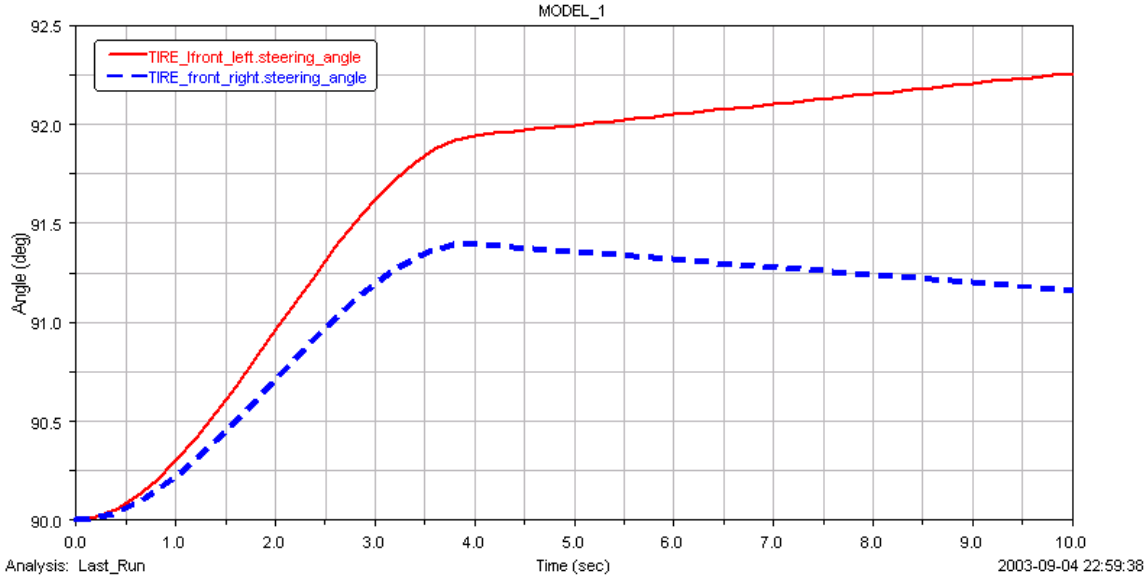


Figure 7.8 Comparison of front steering angles

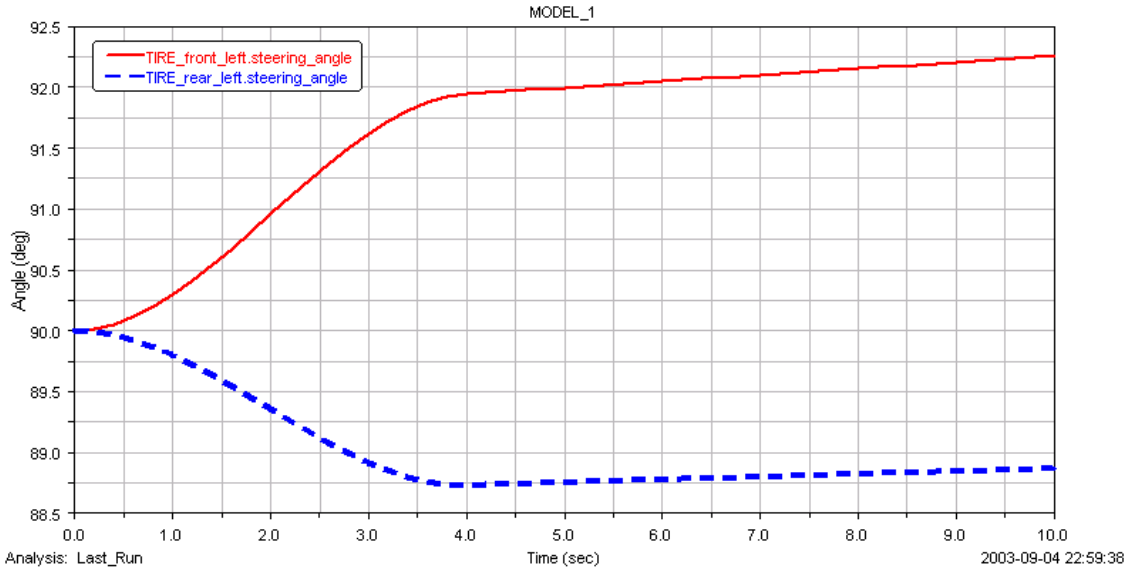


Figure 7.9 Comparison of front left and rear left steering angles

The lateral and longitudinal accelerations of the front left tire are shown in Figure 7.10.

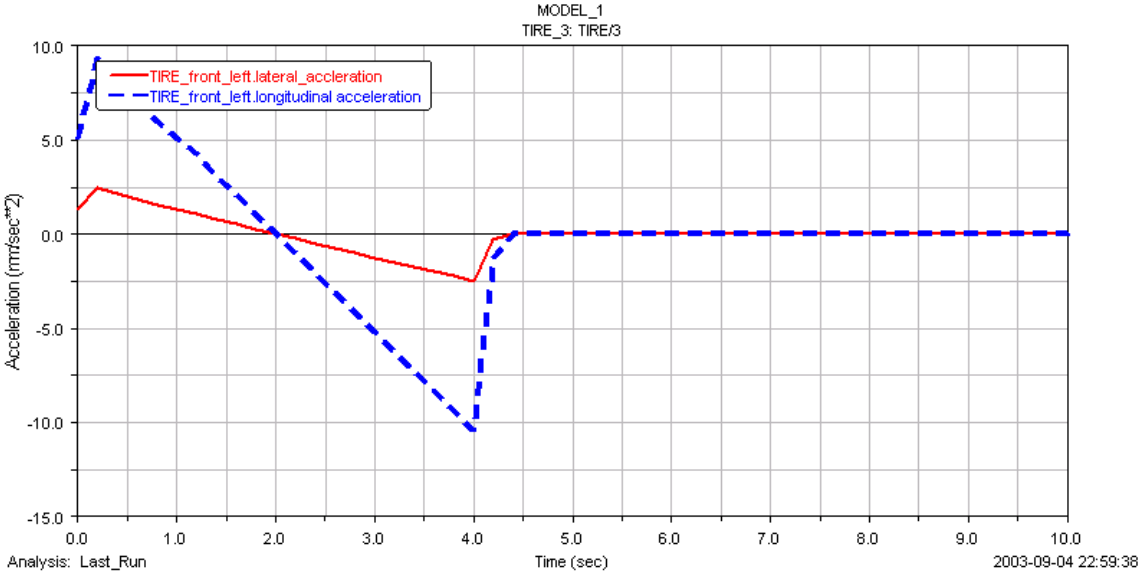


Figure 7.10 Comparison of lateral and longitudinal accelerations

2) $K_s = 0.6$, harmonic sin function is used as input

$$x = A\sin(\omega t)$$

where $A$ represents amplitude and $\omega$ represents frequency of the sine wave input as shown in Figure 7.11.

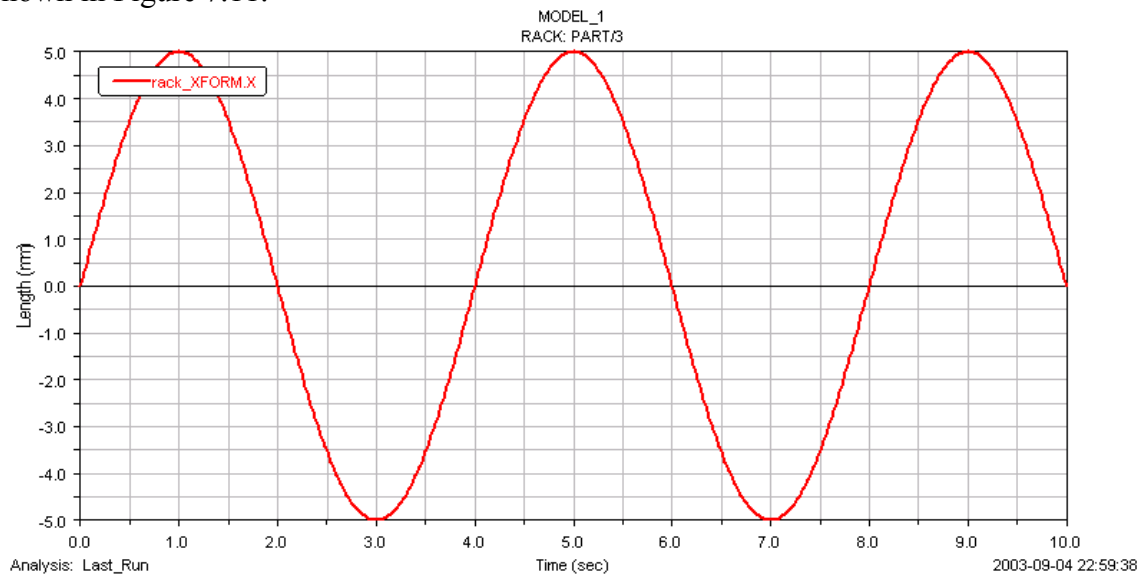


Figure 7.11 Rack displacement (Simple harmonic)

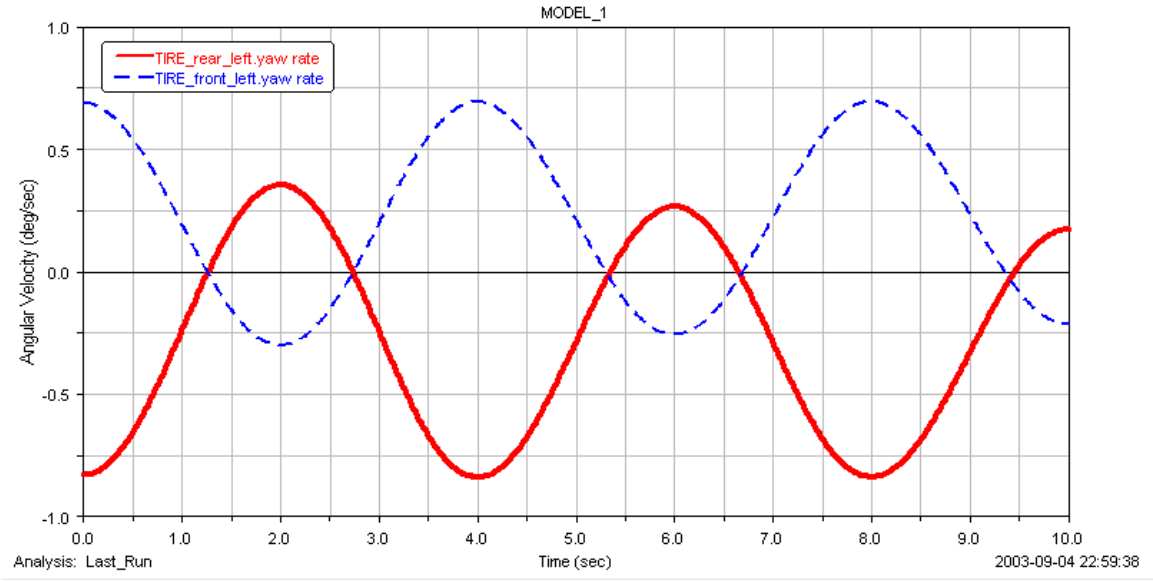


Figure 7.12 Yaw rate comparison (front and rear)

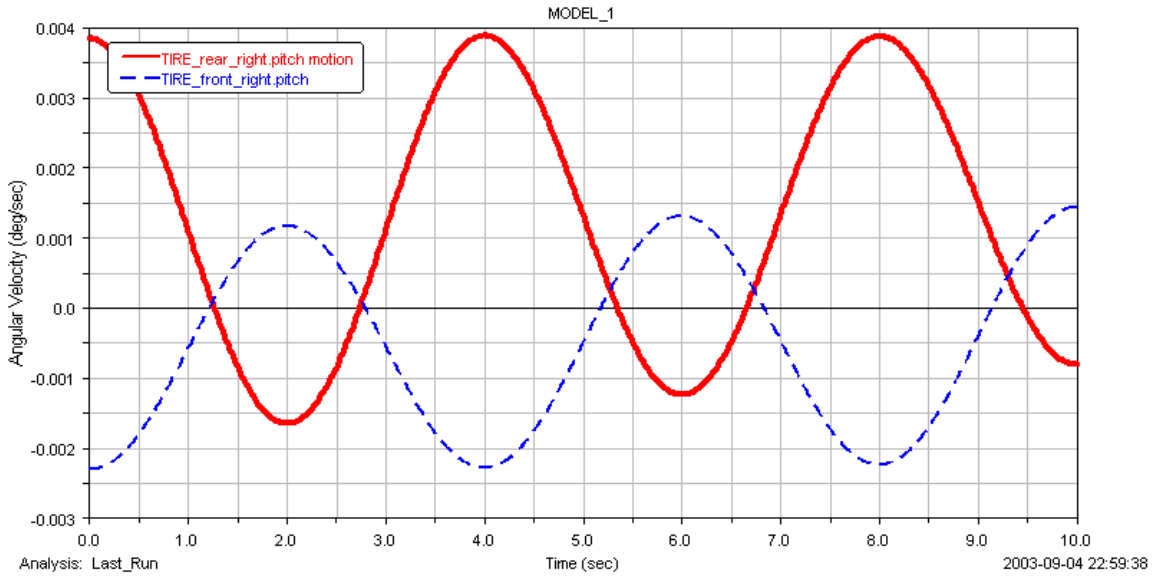


Figure 7.13 Pitch rate comparison (front and rear)

It was also observed that as the frequency of oscillation was increased, steering system failure occurs. This is evident from that fact tie rod joint forces become high making the system unstable, as shown in Figure 7.14.

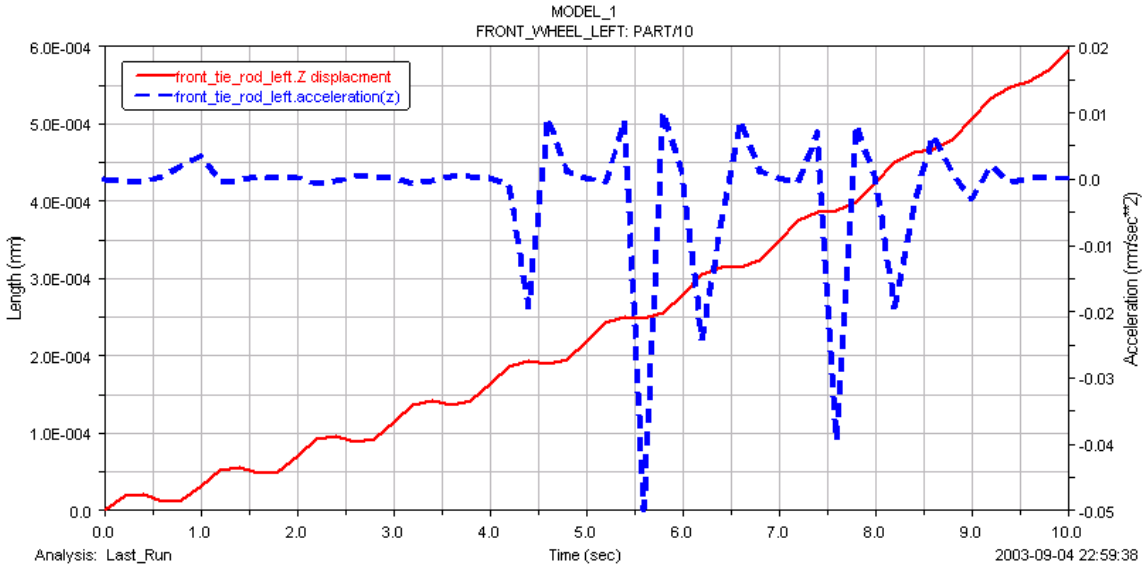


Figure 7.14 Tie rod lift off

# CHAPTER 8

# CONCLUSION

A skid steer model was developed analytically and then dynamic analysis was performed in ADAMS. From the results, it is seen that skid steer causes excessive slip in tires, thereby demanding more power input. At the same time, it allows zero point turn radius which is impossible in other classes of steering systems. Considering the nature of the terrain on which XUV operates, power requirements will be high and tire wear will be greater. This system is suitable for smaller robots which operate on prepared terrain.

A four wheel steering scheme was discussed. Mathematical modeling was done for four wheel steering using a bicycle model where the front and rear steering has independent or dependant inputs. A Matlab simulation was performed. From the Matlab simulation, it was observed that the system is unstable in the present configuration.

A Matlab simulation is followed by a full vehicle model with four wheel steering which is close to an actual vehicle model. The ADAMS program for multi – body systems was used for the modeling, analysis, and animation. A rear steering mechanism for 4WS system is proposed and installed for analysis. Then the vehicle's yaw rate, steering angle, roll motion, lateral acceleration, and vehicle stability are discussed. These results form the basis for more complex model development and mechanism design for future research. This thesis is useful in areas such as

1) Different steering schemes for robotic vehicles
2) Analytical treatment of skid steering
3) Dynamic analysis of steering systems in ADAMS

## FUTURE RESEARCH

A skid steer analytical model is to be verified through experiments with the ATRV-Jr robot. From the experimental results, the analytical model can be refined. A basic model for four wheel steering is proposed. The vehicle model developed here is without a suspension system. Suspension characteristics need to be taken into account. At present, Matlab simulations and ADAMS simulations do not match each other sufficiently closely. Hence the mathematical model needs to be modified to take into account roll and pitch motion. The four wheel steering mechanism discussed will need a controller which will use speed and yaw rate feed back. A detailed design of the steering mechanism and controller will be needed for implementation.

## APPENDIX A: MATLAB CODE FOR SIMULATION OF ROBOT ATRV-JR

```
function ATRV
% Define global variables and time span and initial conditions
global p a1 a2 a3 a4 a5 a6
tspan = [0:0.05:30];
y0 = [0; 0; 0; 0;0;0];

% Solve differential equation using Runge Kutta method
[t,y]=ode45(@f,tspan,y0);

% Trajectory plot
% figure;
% plot(y(:,2),y(:,3))
%plot3 (y(:,2),y(:,3),t);
%axis square, grid on;
% title('ATRV Simulation');
% ylabel('ydot');
% xlabel('xdot');
a0=tspan
a1=y(:,1);
a2=y(:,2);
a3=y(:,3);
a4=y(:,4);
a5=y(:,5);
a6=y(:,6);

figure;
p=polyfit(t,a4,5)
da4 = polyval(polyder(p),t)
plot(t,da4)
title('Vx Vs Time')
xlabel('time')
ylabel('Vx')
grid;
```

```
figure;
q=polyfit(t,a5,5);
da5=polyval(polyder(q),t);
plot (t,da5)
title('Vy Vs Time')
xlabel('time')
ylabel('Vy')
grid;

figure;
plot(da4,da5);
title('Vx Vs Vy')
xlabel('Vx')
ylabel('Vy')
grid;

figure;
r=polyfit(t,a6,5)
da6 = polyval(polyder(r),t)
plot(t,da6)
title('Angular Accn Vs Time')
xlabel('time')
ylabel('Angular Acceleration')
grid

figure;
plot(y(:,4),y(:,5));
title('ATRV Trajectory');
ylabel('Y(t)');
xlabel('X(t)');
grid
figure;
plot(y(:,1),y(:,2))
ylabel('Lateral Velocity');
xlabel('Longitudinal Velocity');
grid;
%figure;
%plot(r13,t);
%axis square, grid on;

% ------------------------------------------------------------------------
```

**Solve first order six linear differential equations**

```
function dydt = f(t,y)
mu = 0.2;
m = 116;
g = 9.81;
I = 20;
mustar = 1 - mu;
b = 0.55;
a = 0.37;
c = mu*m*g/0.1;
t1 = 0.315;
fr = 0.1;
r13 = (a)*abs(y(3)-b*y(1))-(b)*abs(y(3)+a*y(1));
r23 = abs(y(3)-b*y(1))-abs(y(3)+a*y(1));
r45 = 0.49*(abs(y(2)+t1*y(1))+ abs(y(2)-t1*y(1)));
r56 = abs(y(2) +t1*y(1))-abs(y(2)-t1*y(1));
Mr = 2.51*r23 + 0.89*r56;
f1 = 10;%*exp(-t/100);%0.63*(t^3+9);%-0.2*(y(3)^2+y(2)^2);
f2 = -f1;%0.63*%0.63*(exp(-t)+exp(-2*t)+exp(-3*t));
f3 = 2*t1*(f1 - f2)/I;
f4 = 2*(f1 + f2)/m;

dydt = [ f3-Mr
    f4-r45+y(3)*y(1)
    2.13*r13-y(2)*y(1)
    -y(3)*sin(y(6))+y(2)*cos(y(6))
    y(3)*cos(y(6))+y(2)*sin(y(6))
    y(1)];

%--------------------------------------------------------------------------
```

## APPENDIX B: MATLAB CODE FOR VEHICLE HANDLING CHARACTERISTICS AND STEERING SYSTEM SIMULATION

```
% Matlab code for steering system and vehicle handling charactersitics simulation
Nt = 10; % steering Gear ratio
Kt = 10; % motor torque constant
Cs = 50 % damping coefficient of steering system
zeta = 0.5 % mechanical trail
Cf = 2000 %front tire cornering stiffness
Cr =2200; %rear tire cornering stiffness
Ux = 20; %vehicle longitudinal velocity
Uy = 3; %lateral velocity
a = 0.9; % front tire distance
b = 0.9; % rear tire distance
r = 0.0 % yaw velocity rate
Nm = 5; % motor gear ratio
Is = 12; % equivalent moment of inertia of steering system
I = 2000; %vehicle yawing moment of inertia
Im = 10; % motor inertia
C1 = (Nt^2 - 3*zeta*Cf)/Is*Nt*Nm;
C2 = ((Ux/Uy)+(a*r/Ux))/Nt*Nm;
m = 2000; % mass of the vehicle
num = [50];
den = [1 Cs C1 0];
sys = tf(num,den);
% step(sys,100)
% DC Motor Modeling
% R = 0.2
% L = 0.3
% J = 10
% Km =1;
% Kb = 1
% Kf = 0.2
% h1 = tf(Km,[L,R])
% h2 = tf(1,[J,Kf])
% dcm = (h2)*(h1)
```

```
% dcm = feedback(dcm,Kb,1,1);
% sys1 = dcm*sys;
% pole(sys1)
% figure
% step(sys1,100);
% pzmap(sys1)
% figure
% pzmap(sys1)

% Vehicle handling characteristics



a11 = (Cf + Cr)/m*Ux;
a12 = (a*Cf - b*Cr)/m*Ux;
a21 = (a*Cf - b*Cr)/I*Ux;
a22 = (a^2*Cf + b^2*Cr)/I*Ux;
b11 = -Cf/m;
b12 = -Cr/m;
b21 = -a*Cf/I;
b22 = -b*Cr/I;
A = [a11 a12
  a21 a22];
B = [b11 b12
  b21 b22];
C = [1 0
  0 1];

D = [0 0
  0 0];
H = ss(A,B,C,D);
% pole(H)
% pzmap(H)
% step(H,40);


% p=polyfit(t,a6,5)
% da6 = polyval(polyder(p),t)
% plot(da6,t)
% figure;

% Placement of poles for stability of the system
p1 = -10 + 10i;
p2 = -10 -10i;
K = place(A,B,[p1 p2]);
% % % Nbar=rscale(A,B,C,D,K);
```

```
t = 0:0.05:5
% % % % how to give step input
u1=ones(1,length(t));
u2=2*ones(1,length(t));
u = [u1;u2]

x0 = [0 10];

sys_cl=ss(A-B*K,B,C,0);
% % % lsim(sys_cl,Nbar*u,t);
% lsim(sys_cl,u,t,x0);
%--------------------------------------------------
% To convert SS to transfer function
% iu = 1 or 2
% [num, den] = ss2tf(A,B,C,D,iu)
% step input u = 0.001*ones(size(t));

%--------------------------------------------------
[Y,T,X] = LSIM(sys_cl,u,t,x0) ;
lsim(sys_cl,u,t,x0)
a1 = X(:,2)
figure;
p=polyfit(T,a1,5)
da1 = polyval(polyder(p),T)
plot(T,da1)
title('Angular Accleration Vs Time')
xlabel('time')
ylabel('Angular Acceleration')
grid;
```

## APPENDIX C: MATLAB CODE FOR FOUR WHEEL STEERING CHARACTERISTIC CURVE

```
M = 2000;
 a = 0.9;
 b = 0.99;
 L = a+b;
 Cr = 1000;
 Cf = 1200;
 Ux = 0:1:20;
 soln=[];
 final=length(Ux);
 for i=1:final,
   current=((M*a*Ux(i)/Cr*L)-b-0.5)/((M*b*Ux(i)^0.45/Cf*L)+a)-Ux(i);
   soln=[soln current];
 end
% num = (M*a*Ux.^2/Cr*L)-b
% den = (M*b*Ux.^2/Cf*L)+a
% Ks = num/den;
% y = Ux.^2/(Ux.^3+Ux.^2);
% plot (Ux,num,Ux,den)
 plot(Ux,soln)
 xlabel('Speed miles/hr')
 ylabel('steering ratio rear/front')
 grid on
```

## REFERENCES


[1] Luca Caracciolo, Alessandro De Luca, and Stefano Iannitti, "Trajectory tracking of Control of 4 wheel differential driven mobile robot" 1999 IEEE, International conference on Robotics and Automation, Detroit, Michigan.

[2] Peeroon Ramanata and Mehdi Ahmadian, "Optimal Vehicle path Generator using optimization methods" Thesis, Department of Mechanical Engineering, Virginia Polytechnic Institute, April 98.

[3] Thomas D. Gillespie, "Fundamentals of Vehicle Dynamics" Third Edition, S. A. E.

[4] Pradeep Setlur, Dr. John Wagner, Dr. Darren Dawson, and Lance Powers, "A Hardware-in-the-Loop and Virtual Reality Test Environment for Steer-by-Wire System Evaluations" Proceedings of American Control Conference , Denver CO June 2003.

[5] J. Y. Wong, "Theory of Ground Vehicles" 3rd Edition.

[6] "Vehicle steering study" Degree Project by Sebastien Feve and Alexandre Huret D Georgia Institute of Technology , June 1999.

[7] Shin-ichiro Sakai, Hideo Sado, and Yoichi Hori, "Motion Control in an Electric Vehicle with 4 Independently Driven In-Wheel Motors" IEEE Trans. on Mechatronics, Vol. 4, No.1, pp.9-16, 1999.3.

[8] Hongchu Qiu, Qin Zhang, John F. Reid, and Duqiang Wu, "Modeling and simulation of electro-hydraulic steering system" Paper No.: 993076, ASAE Meeting Presentation UILU-ENG-99-7019.

[9] Benjamin Shamah, Michael D. Wagner, Stewart Moorehead, James Teza, and David Wettergreen, "Steering and Control of a Passively Articulated Robot" Sensor Fusion and Decentralized Control in Robotic Systems IV, Vol. 4571, October, 2001.

[10] Woongsnag Jeong, Jinhee Jang, and Changsoo Han, “Modeling and Analysis of four wheel steering vehicle” International ADAMS conference 1994 , Paper 5.

[11] Paul Yih and J. Christian Gerdes, “Modification of Vehicle Handling Characteristics via Steer-by-Wire” American Control Conference Denver, CO 2003.

[12] David M. Brienza and Clifford E.Brubaker, “A steering linkage for short wheelbase vehicles: Design and evaluation in a wheelchair power base” Journal of Rehabilitation and Development Vol 36, No 1 January 1999.

[13] Takashi Ohta Tetsushi Mimuro and Jaekwan Lee, “Robust Lateral Control System with Steering torque Assist” Advanced Electrical/Electronics Department, Car Research & Development Office, Mitsubishi Motors Corporation Cartoronics R&D Center, Association of Traffic and Safety Sciences , Vol 26, No 2 , 2001.

[14] Ben Shamah, Dimi Apostolopoulus, and Michael Wagner “Effect of Tire Design and Steering Mode on Robotic Mobility in Barren Terrain”, William “Red” Whittaker Field Robotics Center, The Robotics Institute Carnegie Mellon University, Proceeding of the International Conference on Field and Service Robots, August, 1999, pp. 287-292.

## BIOGRAPHICAL SKETCH

Shailesh Lakkad was born on December 15, 1975 in Kolhapur, (Maharashtra) India. He obtained his Bachelor's in Mechanical Engineering from University of Pune, India. He obtained the degree with first class with Distinction. While at University of Pune, Shailesh gained valuable experience through the Cooperative Education Program by working at Kirloskar Oil Engines Ltd, Pune India. After graduating, he worked with Bajaj Auto for 3 years. Bajaj Auto Ltd. is one of the largest manufacturers of two and three wheelers in India. He gained experience in reliability support engineering, product development, engine testing etc. After 3 years work at Bajaj Auto, he pursued a masters degree at Florida State University. During his graduate studies, he assisted Dr. Alvi in Thermal Fluid laboratory experiments. He worked as a Research Assistant under Dr. Patrik Hollis. In September 2003, he earned his Masters degree in Mechanical Engineering. Then he moved to Columbus, Indiana to work for Cummins Inc. Ltd, as Design Engineer in Mid Range Customer Engineering Department.